UNIVERSITY OF BIRMINGHAM
University of Birmingham Research at Birmingham

Design, modelling and optimisation of a batch reverse osmosis (RO) desalination system using a free piston for brackish water treatment

Park, Kiho; Burlace, Liam; Dhakal, Nirajan; Mudgal, Anurag; Stewart, Neil A.; Davies, Philip A.

DOI:
10.1016/j.desal.2020.114625

License:
Creative Commons: Attribution-NonCommercial-NoDerivs (CC BY-NC-ND)

Document Version
Publisher's PDF, also known as Version of record

Citation for published version (Harvard):
Park, K, Burlace, L, Dhakal, N, Mudgal, A, Stewart, NA & Davies, PA 2020, 'Design, modelling and optimisation of a batch reverse osmosis (RO) desalination system using a free piston for brackish water treatment', *Desalination*, vol. 494, 114625. https://doi.org/10.1016/j.desal.2020.114625

Link to publication on Research at Birmingham portal

General rights
Unless a licence is specified above, all rights (including copyright and moral rights) in this document are retained by the authors and/or the copyright holders. The express permission of the copyright holder must be obtained for any use of this material other than for purposes permitted by law.

•Users may freely distribute the URL that is used to identify this publication.
•Users may download and/or print one copy of the publication from the University of Birmingham research portal for the purpose of private study or non-commercial research.
•User may use extracts from the document in line with the concept of 'fair dealing' under the Copyright, Designs and Patents Act 1988 (?)
•Users may not further distribute the material nor use it for the purposes of commercial gain.

Where a licence is displayed above, please note the terms and conditions of the licence govern your use of this document.

When citing, please reference the published version.

Take down policy
While the University of Birmingham exercises care and attention in making items available there are rare occasions when an item has been uploaded in error or has been deemed to be commercially or otherwise sensitive.

If you believe that this is the case for this document, please contact UBIRA@lists.bham.ac.uk providing details and we will remove access to the work immediately and investigate.

Download date: 05. May. 2023

Desalination 494 (2020) 114625

Contents lists available at ScienceDirect

Desalination

journal homepage: www.elsevier.com/locate/desal

Design, modelling and optimisation of a batch reverse osmosis (RO) desalination system using a free piston for brackish water treatment

Kiho Park[a], Liam Burlace[a], Nirajan Dhakal[b], Anurag Mudgal[c], Neil A. Stewart[d], Philip A. Davies[a,*]

[a] School of Engineering, University of Birmingham, Edgbaston, Birmingham B15 2TT, United Kingdom
[b] Department of Water Supply Sanitation and Environmental Engineering, IHE Delft, West Vest 7, 2611 AX Delft, the Netherlands
[c] Department of Mechanical Engineering, School of Technology, Pandit Deendayal Petroleum University, Gandhinagar, Gujarat 382007, India
[d] Modus Research and Innovation Limited, Software Centre, Dundee Technology Park, Dundee DD2 1TY, United Kingdom

GRAPHICAL ABSTRACT

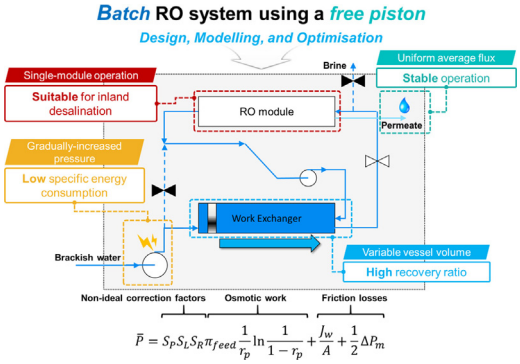

ARTICLE INFO

Keywords:
Batch reverse osmosis
Modelling
Groundwater
High recovery
Energy efficiency

ABSTRACT

Batch RO is a concept for achieving the minimum possible energy consumption in desalination, even at high recoveries. We present a batch RO design that operates cyclically in two alternating phases. The system uses a free piston, housed in a pressure vessel, to transfer pressure from the feed fluid to the recirculating fluid. No complete design procedure for this configuration currently exists. To fill this gap, we present a systematic model based on justified assumptions. The specific energy consumption (SEC) is broken down into contributions from the feed pump, recirculating pump, and auxiliary loads. The calculation of feed pump SEC includes three non-ideal correction factors: concentration polarisation, longitudinal concentration gradient, and salt retention. The model requires only the solution of explicit algebraic equations, without need of specialised numerical techniques, and is implemented in a simple 3-step procedure. The model is applied to an example involving desalination of brackish water using an 8-inch spiral-wound RO module. The design parameters are explored and optimised in a sensitivity analysis. The results show that the optimised batch RO at 80% recovery can produce fresh water with low-energy consumption, achieving 2nd law efficiency of 33.2% compared to 10–15% for conventional brackish water RO.

* Corresponding author.
E-mail address: p.a.davies@bham.ac.uk (P.A. Davies).

https://doi.org/10.1016/j.desal.2020.114625
Received 5 May 2020; Received in revised form 10 July 2020; Accepted 20 July 2020
0011-9164/ © 2020 The Authors. Published by Elsevier B.V. This is an open access article under the CC BY-NC-ND license (http://creativecommons.org/licenses/BY-NC-ND/4.0/).

1. Introduction

Desalination technology has been developed to tackle the growing water shortage by harvesting freshwater from non-conventional resources [1–4]. Such resources include seawater, brackish groundwater and industrial effluents. Given the abundance of these resources, sustainable desalination technology could supply almost unlimited quantities of freshwater to meet municipal and irrigation needs [5].

Most desalination technologies fall in two main groups: thermal-based and membrane-based desalination. Over the last 20 years, the affordability and performance of membrane-based desalination have improved considerably, thanks to advances in membrane technology, pumps and energy recovery devices (ERD) [3,6,7]. Thus, membrane-based technology is rapidly supplanting the older thermal technologies (multi-stage flash and multi-effect distillation) and is considered the most promising approach to desalination system nowadays.

Reverse osmosis (RO) is the most commonly utilised membrane desalination technology. The RO process is simple, easy to scale-up, and has relatively high energy-efficiency among desalination technologies [8,9]. However, recent progress in RO has reached a certain plateau in energy-efficiency, because of the technological maturity of membranes, pumps and ERD [3,4,7]. Nevertheless, the specific energy consumption (SEC) of RO remains above the theoretical minimum work of separation based on the 2nd law of thermodynamics. The main reason for this gap is the irreversibility associated with high pumping pressure in conventional, continuous RO [4,10–12]. High pumping pressure arises partly from the need to continuously exceed the osmotic pressure at the system outlet, which is higher than at the system inlet.

Batch and semi-batch RO systems are prominent candidates for minimising the irreversibility associated with the high pumping pressure [12–18]. Their advantages are most significant at high recovery which is an important objective in many applications. It is important, for example, in desalination of brackish groundwater to minimise groundwater extraction and reduce brine discharge. It is also interesting in seawater desalination, if the aim is to concentrate the brine and recover minerals from it. Further applications requiring high recovery occur in water reuse and volume reduction of industrial and mining effluents. The current growing interests in groundwater conservation, environmental protection, circular economy, and zero liquid discharge, are important drivers to improve and implement low energy or renewable energy powered high-recovery desalination technologies such as batch RO [19–21].

Batch RO and semi-batch RO are cyclic processes that moderate pressure and energy usage by operating at a time-averaged feed pressure below the constant pressure needed in single-stage conventional RO. Rapid recirculation in batch and semi-batch systems leads to a nearly uniform distribution of osmotic pressure throughout. Instead of varying spatially, the pressure varies temporally during the cycle of operation, reaching the same peak value as in conventional RO but with lower average value. The difference between batch and semi-batch RO lies in the details of the design, whereby the batch arrangement keeps the feed water separate from the recirculating water. This separation provides a thermodynamic advantage [12,18]. Separation is achieved using a moving partition, such as a diaphragm, bladder or piston [12,15,17,22–24].

Batch filtration is an ancient artisanal process used in fruit presses, oil presses, and cheese making. But the modern application of batch RO filtration in a scalable industrial design is only recently gaining interest. One of the first publications in this area was the patent by Szucz and Szucs [25] which described 12 embodiments of semi-batch and batch RO systems. The batch RO designs presented therein were complex, using 3 pumps and at least 9 valves. To our knowledge these systems were never built.

Minimisation of complexity of the batch RO design is important – not only to save costs and improve reliability – but also to improve performance. Valves and interconnecting pipelines introduce parasitic loads and dead volumes that compromise efficiency and recovery. For these reasons, a simplified design is preferred. Two types of practical design have been recently been presented in the literature – one using a bladder [22–24] and the other a free piston [26,27]. This article describes and analyses a simple free-piston design with enhanced output.

A batch RO cycle typically comprises three phases: pressurisation, purge, and refill [15]. (Alternatively, these have been named 'permeate production', 'flush' and 'recharge' phases respectively [24]). Though batch RO is theoretically more efficient than continuous RO, a downside is that not all three phases of its cyclic operation are productive. Only the pressurisation phase yields an output, whereas subsequent purge and refill phases do not. Therefore, in a comparison between batch and continuous RO based on equal output per membrane area, the permeate water flux in the batch process will be higher. This causes a penalty in SEC, diminishing the advantage over continuous RO [28]. It is therefore important to minimise the downtime associated with the non-productive purge and refill phases. The free-piston design presented here achieves this by combining these as one simultaneous 'purge-and-refill' phase. Hence there are just two alternating phases: (1) pressurisation (2) purge-and-refill. This latest free-piston design uses only two pumps and three valves. Though a previous article outlined the design, there has been no complete description or analysis of its operation yet [26,27]. The current paper fills this gap.

Besides the complexity of some designs, another hindrance to the adoption of batch RO has been the lack of design procedures. The basic design equations for conventional RO are well known and widely disseminated. Consequently, there are hundreds of companies around the world successfully designing and making conventional RO systems. In contrast, it is likely that only a handful of people have access to the knowledge and expertise to design properly a batch RO system.

The basic formulae for analysing the performance of batch RO are simple in the ideal case. For example, the ideal SEC of batch RO treating a dilute feed solution of osmotic pressure π, is given by [16,29]:

$$SEC_{ideal} = \frac{\pi}{r} \ln \frac{1}{1-r} \tag{1}$$

where r is the recovery. When, however, the analysis includes non-idealities it becomes more complex. Given the unsteady nature of batch RO, systems of non-linear differential equations with time dependent terms have been used for an in-depth analysis [28]. To tackle this complexity, Wei et al. [24] have presented a numerical discretization scheme to model a bladder batch RO system. Swaminathan et al. [28] presented a numerical model for a batch RO system using a non-pressurised feed tank together with an ERD. So far, however, an accessible model for the 2-phase free-piston design of batch RO is lacking.

With the general aim bringing batch RO closer to general adoption, the current work has the following objectives:

1. Describe and explain the design and operation of a free-piston batch RO desalination system that operates in two phases using just 3 valves and 2 pumps.
2. Present a model and a design procedure for the sizing of this system to meet target performance (i.e. output, SEC, recovery and rejection) using explicit algebraic equations applied in a stepwise procedure.
3. Apply the model to a specific case of brackish groundwater desalination and evaluate its performance.

Regarding objective 3, brackish groundwater desalination is chosen for the design case study, because of the scope for efficiency improvement. The energy efficiency of brackish water RO is currently low, approximately 10–15% as measured by 2nd law efficiency, compared to 25–35% in seawater RO where recovery is usually low (< 50%) [30]. Groundwater treatment typically requires high recovery (> 70%) which is a key advantage for batch RO. To show the contribution of the current work, Table 1 summarises the recent studies on batch RO.

Compared to the previous works, this paper is novel in providing a

Table 1
Summary of studies of batch RO system.[a]

Operation type	Feed	Scale	Main topics	Model equations	Ref.
Free piston	Brackish	8-inch SWM (sim)	Design methods for large-scale system, rigorous modelling with algebraic equations	Algebraic equations	This work
Free piston	Brackish	4-inch SWM (exp)	Experimental validation, energy evaluation	N/A	[18]
Forced piston	Brackish	2.5-inch SWM (exp)	Longitudinal dispersion, salt retention, concentration polarisation	Algebraic equations	[15,17,31]
Free piston	Brackish	2.5-inch SWM (exp)	Design configurations compared, preliminary experiments	Algebraic equations	[26,27,32]
Flexible bladder	Brackish, seawater	Not defined (sim)	Model development, energy analysis	Discretized ODE	[12]
Flexible bladder	Seawater	2.5-inch (exp) and 8-inch (sim) SWM	Experimental validation, evaluation of salt retention	Discretized ODE	[23,24]
Modified batch with PX	Seawater	8-inch SWM (sim)	Model development, operational strategy	Discretized PDE	[28]
Ideal batch	Brackish	Not defined (sim)	Model development, concept design, energy analysis	Algebraic equations	[16,33]
Modified batch with PX	Brackish, seawater	Not defined (sim)	Model development, concept design, energy analysis	Discretized ODE	[13]

[a] SWM: spiral wound module; ODE: ordinary differential equation; PDE: partial differential equation; PX: pressure exchanger; sim: simulation; exp.: experiment.

complete design procedure for batch RO, using a mathematical model represented by algebraic equations. The structure of the paper is as follows. Section 2 gives the background to the design of the batch RO. It introduces the important components and explains how the system operates. Section 3 develops the model equations, starting from the idealised performance of Eq. (1), and explains how these are used to design a batch RO system to meet target performance parameters. Section 4 applies the design procedure to the brackish groundwater example, including sensitivity analysis and optimisation. Section 5 summarises the findings and general implications for the future design and applications of the system.

2. The free-piston batch RO design concept

2.1. Background

The free-piston batch RO concept evolved from an earlier forced-piston version in which a Rankine cycle generated the force to drive the piston [31,34]. The free piston is driven by pressurised water from an electrical pump, instead of by the Rankine cycle. Compared to the forced piston, the free piston is easier to seal, because the pressure is almost equal across it. Four free-piston designs have been built and operated as pilot studies, covering various options of single-acting vs. double-acting design, and 2- and 3-phase operation [18,26,27,32,35]. The single-acting, 2-phase design was selected for further development because it offered the best combination of performance and simplicity. It has been demonstrated that this design can be scaled up to a system containing several RO modules in a parallel arrangement [26].

2.2. Description

The preferred free-piston design comprises a feed pump, a recirculation pump, a RO module (comprising a pressure vessel housing one or more membrane elements), a work exchanger vessel housing the free piston, and three 2-way on/off valves. Fig. 1 illustrates its two phases of operation.

In the pressurisation phase, the feed pump generates high pressure to drive permeate through the RO membrane. The pressure is transferred to the recirculating solution via the free piston as it slides horizontally inside the work exchanger vessel. The pressurised feed solution is then fed to the RO module. Downstream of the RO module, brine flows back to the work exchanger via the recirculation pump, thus completing the batch RO loop. As water permeates the RO membrane, salt is retained, and the concentration of the solution inside the loop gradually rises. Thus, the high-pressure pump must supply a gradually increasing pressure to overcome the increasing osmotic pressure. When the piston reaches the right-hand end of the work exchanger, the pressurisation phase ends and purge-and-refill begins. The permeate output equals the batch swept volume (V_{b0}), which is equal to the cross-sectional area of the piston times its displacement (Fig. 1a). Assuming that the water is of constant density independent of pressure and concentration, and that the system is rigid providing constant internal volume, V_{b0} is also equal to the volume of feed water supplied during pressurisation.

The purpose of the purge-and-refill phase is to dispose of the concentrated brine remaining inside the system and refill it with feed solution ready for the start of the next cycle. These purge and refill steps take place simultaneously. The piston moves to the left end of the work exchanger as the recirculation pump transfers the solution to the right side of the piston (Fig. 1b). Meanwhile, the high-pressure pump (operating now at low-pressure) supplies feed solution to purge the brine (volume V_{pg}) remaining inside the pipes and the RO module. This solution is discharged via the purge valve at the right end of the RO module. However, the retained pipe volume ($V_{pipe,R}$) is not purged and has a negative impact on the energy consumption of the batch RO because it contributes to salt retention (see Section 3.3). When the concentration of the exiting brine falls below a threshold level, the purge valve closes, and the purge-and-refill phase finishes, and the pressurisation phase starts again. (Qiu and Davies [15] showed that the optimal threshold is when the decrease in exit brine concentration is half the maximum decrease that would occur if purging continued indefinitely). During the purge-and-refill phase, the feed pressure is insufficient to overcome osmotic pressure – so there is no permeate output. (There may even occur a small backflow due to a forward osmotic effect [24], but this analysis ignores backflow due to the small amount of water flux [36]). The volume of water fed to the system during purge-and-refill equals $V_{pg} + V_{b0}$.

3. Model development and design procedure

In general, key performance parameters of any RO system include output, recovery, SEC, and rejection. The model calculates these parameters for the free-piston batch RO system specifically. It allows the sizes and specifications of the main components to be chosen to meet target values of these parameters.

The model covers all important aspects influencing the performance of the batch RO system, including concentration polarisation and salt retention. It also includes interconnecting pipes. The model makes certain linearizing approximations. For example, it assumes a linear relation between salt concentration and osmotic pressure, following the van't Hoff law. This is an accurate assumption for NaCl concentrations below about 100 kg/m^3 as the osmotic coefficient is almost constant in this range [37–39]. Therefore, it is a good approximation for brackish water treatment, even at high recoveries. The model also assumes linear dependence of permeate water flux on net driving pressure, which has been observed at pressures up to 50 bar [6]. As such, the model makes use of the widely used solution-diffusion model [40,41]. The model further assumes a linear increase of salt concentration along the length

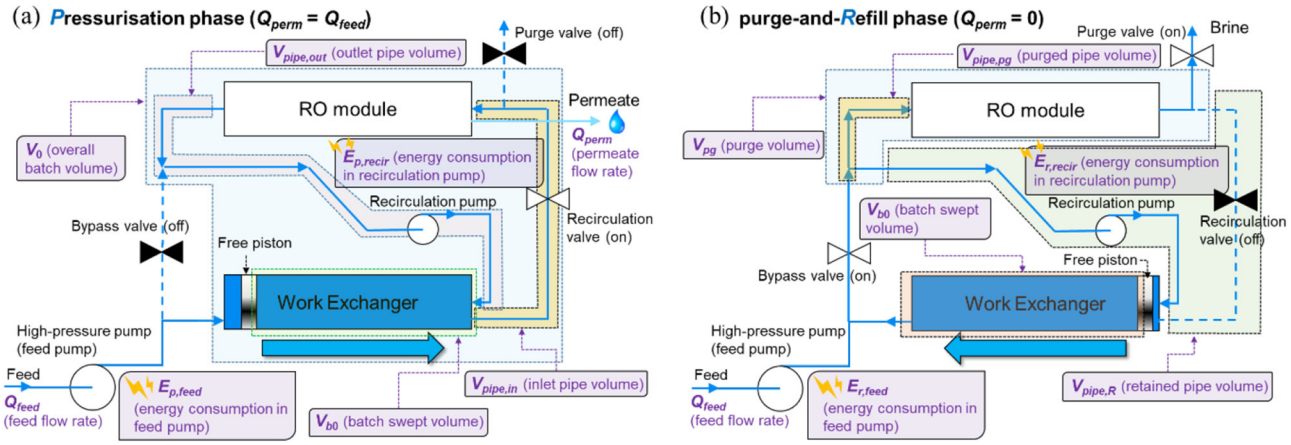

Fig. 1. Schematic of main components and variables in the batch RO system. (a) pressurisation phase and (b) purge-and-refill phase. Solid lines denote active pipes, while dashed lines denote inactive pipes.

of the RO module. This linear increase has been observed for RO modules containing not more than 3 elements in series [42], which is typically the case in batch RO, where shorter RO modules and parallel arrangements are preferred to minimise recirculation pump work. These assumptions enable use of explicit algebraic equations following fundamental principles such as the van't Hoff law and mass balance. Not only do such equations simplify the application of the model, they also help identify and explain the general influence of design parameters on performance and design characteristics.

One aspect that the model does *not* cover in detail is the time decay in performance due to fouling and scaling. There are reasons and evidence to suggest that batch RO system will have better tolerance to fouling and scaling than conventional RO [43], but this aspect is reserved for future models and experimental studies. In this paper, the effects of fouling and scaling are considered at a preliminary level, through the inclusion of a sensitivity analysis in which permeabilities are varied (Section 4.3.4).

Next, we present the model equations and explain how they are applied to each performance parameter. Then we will outline the design and optimisation procedure using the model.

3.1. Output $\overline{Q}_{perm}$ and membrane sizing

After a few initial cycles, the system will reach a steady periodic state such that conditions repeat from one cycle to the next. The analysis therefore considers one cycle as being representative of many cycles. Similarly, the analysis of other reciprocating piston machines, such as internal combustion engines and air compressors, is typically based on just one cycle [44,45].

The sizing calculation considers the relation between recovery r and the flows of feed and permeate (Q_{feed} and Q_{perm}). Recovery is defined as the volume of permeate output divided by the volume of feed input over one full cycle (i.e. including both pressurisation and purge-and-refill phases).

$$r = \frac{V_{perm}}{V_{feed}} \tag{2}$$

Averaging over the cycle duration t_{cycle} gives r in terms of the *average* permeate and feed flows, $\overline{Q}_{perm} = V_{perm}/t_{cycle}$ and $\overline{Q}_{feed} = V_{feed}/t_{cycle}$ respectively:

$$r = \frac{\overline{Q}_{perm}}{\overline{Q}_{feed}} \tag{3}$$

Next, we consider possible variations in flow throughout the cycle. Permeate flows during the pressurisation phase only; brine flows during the purge-and-refill phase only; while feed flow occurs throughout both phases (Fig. 1). Following the analysis of Thiel et al. [46], we choose a constant permeate flux (and therefore constant flow Q_{perm}) during the pressurisation phase to minimise irreversibility. This requires constant feed flow Q_{feed} during pressurisation, because $Q_{perm} = Q_{feed}$ throughout this phase. For efficient constant-speed operation of the feed pump, we keep Q_{feed} unchanged throughout the purge-and-refill phase also, making Q_{feed} constant throughout the whole cycle such that $\overline{Q}_{feed} = Q_{feed} = Q_{perm}$. Permeate flow, however, is not constant, becoming zero during purge-and-refill phase. Therefore, its average value is less than the value Q_{perm} reached during pressurisation phase, according to the recovery:

$$\overline{Q}_{perm} = \overline{Q}_{feed} r = Q_{perm} r \tag{4}$$

(obtained by rearrangement of Eq. (3)). The permeate flow is the product of membrane area A_m and the flux J_w of water through it, thus:

$$Q_{perm} = A_m J_W = \overline{Q}_{perm}/r \tag{5}$$

Given a certain target output $\overline{Q}_{perm}$ and recovery r, the design procedure uses an initial assumption of permeate flux to get an initial estimate of the area of membrane required based on Eq. (5). In practice, membrane elements are only available in standard sizes (e.g. 4-in., 8-in. etc), so a whole number of standard elements must be chosen to meet or exceed the target.

3.2. Recovery r and size of the work exchanger V_{b0}

The geometry of the system determines its recovery. A higher recovery requires a larger work exchanger vessel in relation to the size of the RO pressure vessel. This subsection explains how to proportion the system to achieve the desired recovery. The analysis considers both the major and minor internal volumes shown in Fig. 2.

Eq. (2) can be rewritten to express recovery in terms of internal volumes. As explained in Section 2, permeate output occurs during pressurisation phase only (giving output of $V_{perm} = V_{b0}$), while feed inputs occur during both pressurisation and purge-and-refill phases (requiring feed inputs of V_{b0} and V_{pg} respectively). Thus Eq. (2) becomes:

$$r = \frac{V_{b0}}{V_{b0} + V_{pg}} \tag{6}$$

The value of V_{pg} is determined primarily by the size of the RO membrane element(s). According to the element(s) chosen to achieve the output, V_{pg} is the volume V_m of solution inside the RO membrane element(s), with minor additions for the connecting pipe volume $V_{pipe,pg}$ (including fittings and valves) and the volume V_{ports} associated with the ports of the membrane-containing vessel i.e.

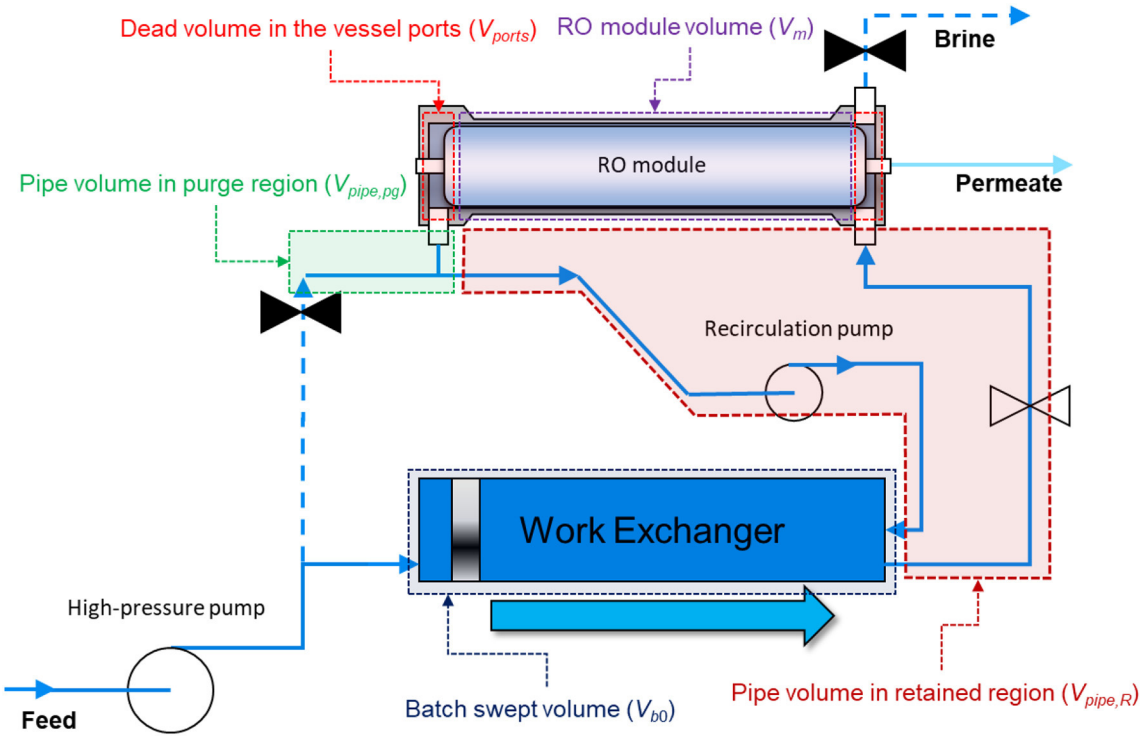

Fig. 2. Volumes of solution in the free-piston batch RO system. The major volumes are the batch swept volume V_{b0} and the volume V_m of solution inside the RO module. The minor volumes are those of the pipes, $V_{pipe,pg}$ and $V_{pipe,R}$.

$$V_{pg} = V_m + V_{pipe,pg} + V_{ports} \tag{7}$$

For a spiral wound element, the solution volume is calculated by considering the membrane channel as rectangular:

$$V_m = A_m H/2 \tag{8}$$

The values of membrane area A_m and channel height H are obtained from membrane manufacturers' data sheets. (Eq. (8) may be modified to deduct feed spacer volume. However, spacer volume is shown to be unimportant in SI Section 7 and is therefore neglected). It is possible also to calculate V_m for other types of RO element such as hollow-fibre or disc elements, but only spiral wound types are considered in this study. V_{ports} is determined from the detailed drawing of the RO pressure vessel and end fittings (see SI Section 1).

Once V_{pg} is known, the required V_{b0} is calculated by rearranging Eq. (1) as:

$$V_{b0} = V_{pg}\frac{r}{(1-r)} \tag{9}$$

Eq. (9) determines the size of the work exchanger, though in practice the actual volume of the work exchanger is slightly bigger than V_{b0} to accommodate the piston. Eq. (9) shows that the work exchanger size is very sensitive to r, being roughly proportional to $1/(1\text{-}r)$ at high recoveries. Thus, increasing recovery from 0.8 to 0.9 roughly doubles the size of the work exchanger vessel. On the other hand, reducing $V_{pipe,pg}$ and V_{ports} helps to minimise its size. Note that $V_{pipe,R}$ does not affect recovery.

3.3. Specific energy consumption (SEC)

The energy consumption per cycle (E) comprises three main components:

$$E = E_p + E_r + E_{aux} \tag{10}$$

Subscripts p, r, and aux denote respectively the pressurisation phase, purge-and-refill phase, and auxiliary loads which are not necessarily specific to either phase. In this study, we only include the energy consumptions in the batch RO, not including energy consumption in pre-treatment units. Thus, the SEC in the batch RO system can be calculated dividing by the water output over the cycle:

$$SEC = \frac{E}{V_{b0}} = \frac{E_p + E_r + E_{etc}}{V_{b0}} = SEC_p + SEC_r + SEC_{aux} \tag{11}$$

Next, we discuss each of these three components in turn.

3.3.1. Energy consumption of the pressurisation phase (SEC_p)

The largest contribution to SEC comes from the pressurisation phase – primarily from the feed pump and secondarily from the recirculation pump. Thus, SEC_p can be expressed as:

$$SEC_p = \frac{E_{p,feed} + E_{p,recir}}{V_{b0}} = SEC_{p,feed} + SEC_{p,recir} \tag{12}$$

The energy consumptions of each pump equal the volume of water displaced, multiplied by differential pressure, and divided by pump efficiency. Differential pressure is required to overcome osmotic and frictional effects. Frictional effects are constant through the cycle, contributing constant differential pressure as the flow is constant. In contrast, osmotic pressure varies over the cycle, and therefore it is appropriate to use the volume-weighted average pressure to calculate SEC [47].

The work to overcome osmotic pressure in the free-piston batch RO machine is $-\int_0^{Vb0} PdV$. (This integral resembles the well-known case of indicated work in other reciprocating machines such as internal combustion engines or reciprocating compressors). Division by the swept volume V_{b0} gives the ideal minimum average pressure over the pressurisation cycle as $\overline{P} = -\int_0^{Vb0} PdV/V_{b0}$. Evaluation of the integral (with the help of the van't Hoff law to give the inverse relation between V and P) leads to the logarithmic expression of Eq. (1) for ideal minimum average pressure (see Appendix A for further details). Specific energy consumption equals $\overline{P}$ in the ideal case of a perfectly efficient feed pump, but with feed pump efficiency η_{feed} included, it will increase according to:

$$SEC_{p,feed} = \frac{1}{\eta_{feed}}\overline{P} \tag{13}$$

The real values of $\overline{P}$ and SEC are higher than Eq. (1) ideally indicates, because of losses caused by concentration polarisation, by longitudinal concentration gradient inside the RO module, by salt retained in the system (which causes the concentration at the start of the pressurisation cycle to be higher than the feed concentration) and by net driving pressure to overcome hydrodynamic resistance in the pores of the RO membrane. There is also a small pressure requirement caused by the cross-flow pressure drop ΔP_m in the RO module. With these factors included, $\overline{P}$ can be expressed as a sum of three terms as follows (assuming that the gauge pressure on the permeate side is zero).

$$\overline{P} = S_P S_L S_R \pi_{feed} \frac{1}{r_p} \ln \frac{1}{1-r_p} + \frac{J_w}{A} + \frac{1}{2}\Delta P_m \tag{14}$$

with

$$\Delta P_m = \frac{L_m f_m \mu v}{(0.5H)^2} \tag{15}$$

$$v = \frac{Q_{recir} + 0.5Q_{feed}}{0.5Hw} \tag{16}$$

where, S_P is the concentration polarisation factor, S_L is the longitudinal concentration gradient factor, S_R is the salt retention factor, π_{feed} is the osmotic pressure of the feed solution (calculated, for example, by the van't Hoff law), r_p is the recovery at pressurisation phase, A is the water permeability of the RO membrane, ΔP_m is the pressure drop in the RO membrane module, f_m is the friction factor inside the RO module, L_m is the RO module length, v is the linear velocity inside the RO module, μ is the solution viscosity, H is the membrane channel height, w is the membrane width, and Q_{recir} is the recirculation flow rate at the exit of the RO module. The first term on the right-hand side of the Eq. (14) is the osmotic pressure amplified by the three correction factors (S_P, S_L and S_R), whereas the second and third terms are frictional. The second term is the net-driving pressure corresponding to hydrodynamic friction for water permeation across the RO membrane. The third term is the average pressure drop in the RO module [48], approximated at the midpoint. (This term could be expanded to include friction losses in the inlet pipework of the RO module; however, these losses are neglected because they are generally very small compared to the pressure supplied by the feed pump).

In addition, the peak pressure $\widehat{P}$ in the batch RO is also important to select an appropriate material and thickness for the pipe. It is calculated by a similar approach, using the following equation:

$$\widehat{P} = S_P S_R \pi_{feed} \frac{1}{(1-r_p)} + \frac{J_w}{A} + \frac{1}{2}\Delta P_m \tag{17}$$

Note that, unlike in Eq. (14), the term S_L is not included. This is because the longitudinal concentration gradient is absent at the beginning and end of the cycle (see Appendix A and Fig. S6 in Supporting information). The value of recovery ratio r_p used in Eqs. (14) and (17) is slightly smaller than the system r. It refers to the volume of recovered water as fraction of the total initial volume inside the batch RO system:

$$r_p = \frac{V_{b0}}{(V_{b0} + V_{pg} + V_{pipe,R})} \tag{18}$$

The difference arises on account of the retained volume $V_{pipe,R}$ that does not get purged from the system during the purge-and-refill phase. If $V_{pipe,R} = 0$, then $r_p = r$.

Concentration polarisation in the batch RO system is a topic of ongoing investigation. Nevertheless, established equations for the concentration polarisation calculation in the continuous RO system are used at this time because the RO module used in the batch RO system is the same spiral-wound type as in the continuous RO system. The equations for concentration polarisation are given below based on the Sherwood analogy [13,49–52]:

$$Re = \frac{\rho v (0.5H)}{\mu} \tag{19}$$

$$Sc = \frac{\mu}{\rho D} \tag{20}$$

$$Sh = 0.20 Re^{0.57} Sc^{0.4} \tag{21}$$

$$k = \frac{Sh \bullet D}{0.5H} \tag{22}$$

$$S_p = \frac{C_m}{C_b} = exp\left(\frac{J_w}{k}\right) \tag{23}$$

In the above equations, ρ is the solution density, k is the mass transfer coefficient, D is the diffusion coefficient of salt in water, and subscripts m and b indicate the membrane surface and bulk solution, respectively. Note that the crossflow velocity v decreases slightly from inlet to outlet, and so the average value is used from Eq. (16). Note also that the characteristic length used the Reynolds and Sherwood numbers (Re and Sh) is half the channel height (equal to the spacer fibre diameter) following Koutsou et al. [50].

The second term in Eq. (14), S_L, has a similar meaning to S_P, except that it represents concentration gradient in the direction of flow rather than perpendicular to it. As explained in Appendices A and B, the ratio of actual work and ideal work (W_{actual}/W_{ideal}) depends on the longitudinal concentration gradient (S_L) inside the RO membrane module. S_L reflects a rise in concentration towards the output of the RO module, because of the finite recirculation flow. It is the concentration of salt in the membrane feed channel, averaged over length and position, divided by the concentration that would occur if the recirculation flow were large enough to achieve uniform concentration longitudinally. The calculation of S_L is based on dynamic modelling of mass balance, with a linear concentration profile assumed in the RO module and homogeneous concentration assumed in the work exchanger vessel (Appendices A and B). Because of this linear approximation, the calculation may be less accurate for long RO modules containing several elements in series. The relation between S_L and the recirculation flow ratio α is:

$$S_L = 1 + G\alpha^{-n} \tag{24}$$

where α is defined as the recirculation flow at the RO module outlet, divided by the permeate flow (or feed flow).

$$\alpha = \frac{Q_{recir}}{Q_{perm}} = \frac{Q_{recir}}{Q_{feed}} \tag{25}$$

Because the intention of the batch RO design is to use a rapid recirculation to homogenise concentration, it is normally expected that α is substantially greater than 1. Eq. (24) is an approximation that fits closely the model in Appendices A and B over the range $1.5 \le \alpha \le 6$. The values of G and n depend on the recovery r (see Table 2 below and Fig. S5).

Table 2
Coefficients in Eq. (24) for S_L depending on the recovery; valid for recirculation flow $1.5 \le \alpha \le 6$.

Recovery r	G	n
0.5	0.03135	0.8312
0.55	0.04018	0.8427
0.6	0.0508	0.8548
0.65	0.06357	0.8673
0.7	0.07897	0.8805
0.75	0.09763	0.8943
0.8	0.1205	0.9087
0.85	0.1492	0.9239
0.9	0.1866	0.9398

The third term in Eq. (14), the salt retention term S_R, represents the fact that the concentration of salt at the start of each cycle is slightly elevated, because excess salt is not completely purged from the system by the end of the previous cycle [15,24]. It is obtained from the mass balance equations (see Appendix C for detailed derivation).

$$S_R = \frac{C_0}{C_{feed}} = \left[\frac{\left(1+\frac{V_{pipe,R}}{V_{pg}}\right)}{1+(1-r)\frac{V_{pipe,R}}{V_{pg}}}\right]\left[1+\frac{r\bullet\lambda}{(1-\lambda)}\right] \tag{26}$$

where C_0 is the initial concentration in the batch RO cycle, C_{feed} is the feed solution concentration, and λ is the longitudinal dispersion factor. The first term in square brackets represents salt retained inside the pipe volume $V_{pipe,R}$ (Fig. 2) and the second term in square brackets represents the salt retained in the RO module. This factor λ represents the amount of salt retained in a RO module, when it is eluted with a volume V_m of clean water, as a fraction of the salt initially contained in the module. In the ideal case, $\lambda = 0$ but due to dispersion effects (e.g. Taylor dispersion) $\lambda > 0$. An earlier experimental study determined that $\lambda = 0.08$ for a spiral-wound RO element; hence $\lambda = 0.08$ is used in this study [15].

All three factors (S_P, S_L and S_R) correct for non-idealities. They have ideal minimum values of 1 and real values slightly above 1, with higher values representing increasing losses.

The recirculation pump also contributes to SEC_p. It compensates the pressure losses caused by the friction inside the RO module, connecting pipes, bends, and valves. The SEC of the recirculation pump in the pressurisation phase is calculated by multiplying its power consumption by the phase duration and dividing by the output volume V_{b0}, thus:

$$SEC_{p,recir} = \frac{\Delta P_{p,recir}\bullet Q_{recir}}{\eta_{recir}\bullet V_{b0}}\frac{V_{b0}}{Q_{feed}} \tag{27}$$

where $\Delta P_{p,recir}$ is the pressure difference across the recirculation pump, Q_{recir} is the recirculation flow rate, and η_{recir} is the recirculation pump efficiency. V_{b0}/Q_{feed} is the elapsed time t_p for the pressurisation phase in each batch RO cycle. Because the recirculation flow rate in the recirculation pump is αQ_{feed}, Eq. (27) can be arranged as:

$$SEC_{p,recir} = \frac{\Delta P_{p,recir}\bullet\alpha}{\eta_{recir}} \tag{28}$$

The $\Delta P_{p,recir}$ is determined by the recirculation flow rate and friction factors in the RO module, pipelines, and fittings. The equation for pressure drop is obtained combining the resistance coefficient method and friction factor inside the RO module, as follows [53–56]:

$$\Delta P_{p,recir} = \Delta P_m + \frac{\rho}{2}\left(f_{pipe}\frac{L_{pipe,in}v_{pipe,in}^2 + L_{pipe,out}v_{pipe,out}^2}{d_{pipe}} + \sum K_i v_i^2\right) \tag{29}$$

where, f_{pipe} is the friction factor in the pipe, which can be calculated from Moody diagram using Reynolds number and relative roughness of the pipe, L_{pipe} is the lengths of the pipes, d_{pipe} is the inner diameter of the pipes, subscripts $_{in}$ and $_{out}$ are the inlet and the outlet pipe sections before and after the RO module as illustrated in Fig. A1 in Appendix A, K_i is the loss coefficient in the i'th fitting or valve; v_{pipe} and v_i are the fluid velocities in the respective pipe sections and fittings (or valve). Various sources are available to calculate K, for example the Darby 3-K method [53]:

$$K = \frac{K_1}{Re} + K_\infty\left(1+\frac{K_d}{{d_{pipe}}^{0.3}}\right) \tag{30}$$

where, K_1, K_∞, and K_d are coefficients for each fitting, such as bends and T-joints. Alternatively, manufacturers of pipe fittings often supply relevant loss factors. This study uses the Darby 3-K method, as it is the most accurate general method for a range of pipe sizes and flow rates.

The quadratic dependence on velocity in Eq. (29) suggests that the pressure drop could become excessive if the pipework is designed badly. To minimise pressure drop, it is desirable to choose a large diameter d_{pipe} for the pipes and fittings; however, large d_{pipe} contributes to larger pipe volumes $V_{pipe,pg}$ and $V_{pipe,R}$, which is detrimental to the recovery and $SEC_{p,feed}$. This trade-off must be considered in the choice of d_{pipe}.

Note that Eq. (29) assumes that the same value of d_{pipe} is used for all the pipes and fittings. If this is not the case, Eq. (29) should be expanded into separate terms for each section of pipe.

3.3.2. Energy consumption of purge-and-refill phase (SEC_r)

The feed and recirculation pumps continue to consume energy during the purge-and-refill stage, but at a different rate because of different conditions. Similar to Eq. (12), SEC in the purge-and-refill phase is given:

$$SEC_r = \frac{E_{r,feed} + E_{r,recir}}{V_{b0}} = SEC_{r,feed} + SEC_{r,recir} \tag{31}$$

There is no need for high pressure in the purge-and-refill phase, as only frictional and no longer osmotic pressure is acting. The displaced volume is the purge volume (V_{pg}) supplied by the feed pump, plus the batch swept volume (V_{b0}) transferred by the recirculation pump. Because the feed flow rate is fixed throughout both phases, the elapsed time for the purge-and-refill phase (t_r) can be calculated as V_{pg}/Q_{feed}. The recirculation flow rate in the purge-and-refill phase is calculated from the elapsed time for the purge-and-refill phase and the amount of volume transferred by the recirculation pump as follows:

$$Q_{r,recir} = V_{b0}\frac{Q_{feed}}{V_{pg}} \tag{32}$$

Then, the SEC_r can be expressed as:

$$SEC_{r,feed} = \frac{\Delta P_{r,feed}Q_{feed}}{\eta_{feed}V_{b0}}\frac{V_{pg}}{Q_{feed}} = \frac{\Delta P_{r,feed}V_{pg}}{\eta_{feed}V_{b0}} \tag{33}$$

$$SEC_{r,recir} = \frac{\Delta P_{r,recir}Q_{r,recir}}{\eta_{recir}V_{b0}}\frac{V_{pg}}{Q_{feed}} = \frac{\Delta P_{r,recir}}{\eta_{recir}} \tag{34}$$

The $\Delta P_{r,feed}$ and $\Delta P_{r,recir}$ can be calculated using the approach of Eq. (29). However, to calculate $\Delta P_{r,recir}$, only pressure drops due to pipelines and fittings need be considered, whereas $\Delta P_{r,feed}$ should also include the cross-flow pressure drop in the RO membrane (see Supporting Information).

3.3.3. Energy consumption of auxiliary loads (SEC_{aux})

Finally, auxiliary energy loads in the batch RO system such as the controller (including sensors) and valves are included, i.e.

$$SEC_{aux} = SEC_{ctr} + SEC_{valves} \tag{35}$$

There are no general formulae for these loads, as they depend on the components chosen and mode of operation. Though generally minor, auxiliary loads can become significant in smaller desalination systems.

3.4. Salt rejection (R_s)

The salt flux through the RO membrane is given by including the non-ideal correction factors in the osmotic pressure term of Eq. (14):

$$J_s = BS_PS_LS_RC_{feed}\frac{1}{r_p}\ln\frac{1}{1-r_p} \tag{36}$$

where B is the salt permeability of the RO membrane. Then, the concentration in the permeate (C_{perm}) and salt rejection R_s (%) in the batch RO are calculated as follows:

$$C_{perm} = \frac{J_s}{J_w} = \frac{B\bullet A_m}{Q_{perm}}S_pS_LS_RC_{feed}\frac{1}{r_p}\ln\frac{1}{1-r_p} \tag{37}$$

$$R_s = 100\left(1 - \frac{C_{perm}}{C_{feed}}\right) = 100\left(1 - \frac{B \bullet A_m}{Q_{perm}} S_p S_L S_R \frac{1}{r_p} \ln \frac{1}{1 - r_p}\right) \quad (38)$$

3.5. Design procedure

It is recommended to carry out the design in three stages as follows:

1. *Approximate design*: The design process is simplified by neglecting the friction and volume of the connecting pipes. The design of the pipes, fittings and valves is a time-consuming process – but only has a somewhat minor effect on the overall performance. It is therefore recommended first to design the system *excluding* the effects of the pipes (i.e. assuming zero pipe volume and friction) to establish an approximate design which estimates the sizes of the RO membrane module and the work exchanger vessel. This design is modelled based on a nominal choice of permeate flux and checked to see that target output, rejection, and SEC are approximated. If not, adjustments should be made to the type and size of membrane and the permeate flux. The peak pressure in the system, which is important for specifying pipes and valves of adequate rating, is established at this first stage.
2. *Baseline design*. With the geometry, flow rates and pressures estimated – the pipes, fittings and valves can be designed to connect the vessels. Pumps are also be specified at this stage. It is generally an iterative process to select the preferred pipe size, taking into account performance, cost and availability. With the pipe friction and volumes included, the baseline design is arrived at. The additional pipe volume ($V_{pipe,pg}$) increases the purged volume V_{pg}; therefore, the swept volume V_{b0} has to be increased slightly in the baseline design to maintain the target recovery r. The model is applied to the baseline design using a nominal choice of recirculation flow (say $\alpha = 3$) to arrive at the baseline performance.
3. *Optimised design*: Iterative application of the model, varying α, then provides the final optimised design for minimal SEC. The optimisation may also re-adjust other input parameters to the model, such as permeate flux and V_{b0}, to fine tune target parameters of rejection, SEC, and recovery. A sensitivity study is useful at this stage to explore the design choices and trade-offs.

4. Design example: treatment of brackish groundwater

In this section, we give a specific example using the above model and design procedure. The aim is to design a pilot-scale batch RO system for brackish groundwater treatment meeting the specifications of Table 3.

4.1. Practical design considerations

Before applying the model, we explain some practical consideration that inform the design choices:

4.1.1. Minimising dead volumes in the RO pressure vessel

In batch RO, it is important to minimise the volumes V_{ports} associated with the ports (Section 3.2). For conventional RO, pressure vessels may have large V_{ports} without affecting performance. In the absence of pressure vessels designed specifically for batch RO, these volumes can be reduced by plastic filling inside the vessel, which is designed to displace the maximum volume of liquid but without restricting flow (see SI Section 1).

4.1.2. Number and type of membrane elements

Most recent studies on batch RO used 2.5- or 4-inch spiral-wound modules [12,16–18,43]. However, the current industry standard in full-scale operation is the 8-inch spiral-wound module [57,58]. Therefore, the 8-inch size was selected here. Eq. (5) estimates the number of RO elements. If several elements are needed, parallel rather than series arrangements are preferred to minimise pressure drop $\Delta P_{p,recir}$. This example uses just one element.

Both high-flux and high-rejection membranes are available. High-flux membranes have higher water permeability, but lower salt rejection. High-rejection membranes can produce higher quality of permeate but require higher pressure and more energy. Information about membrane performance (water permeability A and salt rejection B) can be inferred from published data (see SI Section 1).

4.1.3. Valve type

The batch RO system requires valves to control its operation, with periodic actuation every few minutes. The ideal valve would be fast acting, resistant to salinity, durable and not prone to blockage. It would also have low power consumption and few electrical connections, present low resistance to flow, be readily available and inexpensive. No off-the-shelf valve meets these requirements perfectly. In this study, motorised ball valves were selected for low resistance to flow and low power consumption – although they are more complex and expensive than solenoid valves (see SI for valve pressure drop and power consumption calculations).

4.1.4. Pump types

The feed pump must provide constant flow and maintain its efficiency over a range of pressures, as pressure gradually increases during the pressurisation phase. Centrifugal pumps only maintain efficient operation at the optimum operating point of pressure and flow. As such, they are not ideal for the feed pump. A positive displacement pump is preferred, such as helical rotor type or piston pump. Helical rotor pumps are widely used in groundwater pumping and some are compatible with brackish water. Therefore, a helical rotor type pump was selected. Helical rotor pumps can operate at the required conditions with efficiency of $\eta_{feed} = 70\%$ and this value was used in the calculations. In contrast, the recirculation pump works at constant flow and pressure, making a centrifugal type suitable. Based on data for standard centrifugal pumps, an efficiency of $\eta_{recir} = 50\%$ was assumed.

4.2. Application of design procedure

The procedure follows Section 3 above and is applied next using the high-flux membrane. (For results with the high-rejection membrane see Table S5).

1. *Approximate design*. The approximate design was based on an initial

Table 3
Target parameters for example design.

Parameter	Value	Comment
Osmotic pressure of feed solution π_{feed} [kPa]	237.3	Corresponding to a NaCl solution of concentration $C_{feed} = 3$ kg/m^3 at 25 °C
Operating temperature [°C]	25	Corresponding to a standard test condition
Recovery r [−]	0.8	A high recovery is generally favoured in groundwater treatment to minimise brine and conserve groundwater
Output permeate production rate $\overline{Q}_{perm}$ [m^3/h]	> 0.42	Corresponding to a pilot-scale batch RO system with 8-inch RO module
Water output quality C_{perm} [kg/m^3]	< 0.2	Corresponding to rejection $R_s > 93.3\%$
Target SEC [kWh/m^3]	< 0.5	This improves on most brackish water desalination systems currently available

Table 4
Main parameters of approximate design (neglecting pipes), baseline design (including pipes), and optimised design (recirculation flow optimised to minimise *SEC*) – meeting specifications of Table 3 (one high-flux 8-inch membrane, η_{feed} = 70%, η_{recir} = 50%, f_{pipe} = 0.03008, f_m = 20, λ = 0.08).

Variable	Approximate design (neglecting pipes)	Baseline design	Optimised design	Equations used
Permeate flux J_w [L/m^2/h]	20	22.06	22.06	(5)
Output $\overline{Q}_{perm}$ [m^3/h]	0.654	0.72	0.72	(4)
Feed flow Q_{feed} [$\times 10^{-4}$ m^3/s]	2.267	2.500	2.500	(3), (4)
Recirculation flow α [−]	3.0	3.0	2.0265	(25)
Cycle duration, t_{cycle} [s]	320	322.8	322.8	(2), (3)
Elapsed time in pressurisation phase, t_p [s]	256	258.2	258.2	(27)
Elapsed time in purge-and-refill phase, t_r [s]	64	64.6	64.6	(31)
Number of 8-inch RO module [each]	1	1	1	(5)
Recovery, r [−]	0.8	0.8	0.8	(2), (3)
Recovery at pressurisation phase, r_p [−]	0.8	0.787	0.787	(18)
Pipe volume (purged) $V_{pipe,pg}$ [m^3]	0	0.00037	0.00037	SI
Pipe volume (retained) $V_{pipe,R}$ [m^3]	0	0.00133	0.00133	SI
Port dead volume V_{ports} [m^3]	0	0.00126	0.00126	SI
Purged volume V_{pg} [m^3]	0.0145	0.0161	0.0161	(7)
Work exchanger volume V_{b0} [m^3]	0.0580	0.0646	0.0646	(9)
Cross flow velocity v [m/s]	0.0558	0.0615	0.0444	(16)
Concentration polarisation S_P [−]	1.092	1.097	1.118	(23)
Longitudinal concentration gradient S_L [−]	1.044	1.044	1.063	(24)
Salt retention S_R [−]	1.070	1.139	1.139	(26)
Rejection R_S [%]	94.4	94.7	94.2	(38)
Average pressure $\overline{P}$ [kPa]	827.1	878.1	899.7	(14)
Peak pressure $\widehat{P}$ [kPa]	1631	1661	1687	(17)
SEC_p [kWh/m^3]	0.3417	0.3762	0.3687	(12)
SEC_r [kWh/m^3]	0.0002	0.0052	0.0052	(31)
SEC_{aux} [kWh/m^3]	0	0.0157	0.0157	(35)
SEC_{total} [kWh/m^3]	0.3419	0.3972	0.3896	(11)
SEC_{ideal} [kWh/m^3]	0.1326	0.1295	0.1295	(1)
2nd law efficiency [−]	0.388	0.326	0.332	SEC_{ideal}/SEC_{total}

assumption of permeate flux J_w = 20 L/m^2/h and recirculation ratio α = 3. It showed that one 8-in. module (high-flux type) would readily meet the target output. The output of 0.654 m^3/h was exceeding the 0.42 m^3/h target (see Tables 3 and 4). Based on the membrane parameters in Table S1, the volume of solution inside this module was calculated as V_m = 0.0145 m^3 and a work exchanger vessel size of V_{b0} = 0.058 m^3 was estimated. The peak pressure of 1631 kPa (16.31 bar) exceeded the limit of available polymer pipework, so it was decided to use instead stainless steel pipes to withstand the pressure. At this stage, the calculation of losses neglected pipe friction, but included friction loss ΔP_m in the RO module (with friction factor f_m = 20, see SI). Similarly, salt retention S_R neglected pipes but accounted for the RO module (with λ = 0.08). The approximate design gave a result of *SEC* = 0.3419 kWh/m^3.

2. *Baseline design*. Based on the flows and sizes of the approximate design, the pipework was designed with the help of the Darby 3-K model to determine pressure losses. A 1.25-inch pipe size was preferred, because 1-in. gave a significant SEC penalty whereas 1.5-inch size gave negligible advantage (see SI Section 2.3). The additional volume of the pipework made it necessary to increase V_{b0} by 11% to 0.0646 m^3 to maintain the recovery of r = 0.8. With the pipe details fixed, it was possible to select valves and calculate their power usage, and thus to determine SEC_{aux} (see SI Section 2.4). The baseline design also included V_{ports} that was previously neglected. An adjustment was made to the permeate flux, increasing it from 20 to 22.06 L/m^2/h output, to match the output of the available helical rotor pump (corresponding to 0.9 m^3/h output). The penalty in SEC, including additional friction losses and salt retention, was an increase of 16.2% to *SEC* = 0.3972 kWh/m^3. Nonetheless, this still satisfied the target of *SEC* < 0.5 kWh/m^3. Rejection was 94.7%, meeting the permeate quality target in Table 3.
3. *Optimised design*. The baseline design was satisfactory, but could be further improved by adjusting the recirculation flow to minimise *SEC*. The recirculation flow (as a multiple α of permeate flow) was decreased from α = 3 to α = 2.0265, thus decreasing *SEC* marginally by 1.9% to 0.3896 kWh/m^3 (Table 4). At this optimised condition, the recirculation pump flow was $Q_{p,recir}$ = 5.07 × 10^{-4} m^3/s against a pressure of $\Delta P_{p,recir}$ = 10.3 kPa, with 62.3% of the pressure loss occurring in the RO module and the remainder occurring in the pipe, fittings and valves. Fig. 3a shows how the different *SEC* components contribute to *SEC* as the cycle progresses. The vertical axis represents specific power [kW/m^3] per cycle output V_{b0}, and the horizonal axis represents time [h]. Therefore, the integral below the curve is *SEC* [kWh/m^3]. The largest contribution to *SEC* is from the feed pump during pressurisation $SEC_{p,feed}$, associated with the large pressure it supplies. Fig. 3b shows the applied pressure and the permeate flow rate in a whole batch RO cycle. Because the feed flow rate is assumed at constant, t_p and t_r are determined by r. As mentioned above, only the pressurisation phase is productive, so the permeate flow for the whole cycle should be averaged over both phases. Because most of energy consumption of the batch RO occurs in the pressurisation phase, the applied pressure in this phase should be analysed in more detail. The breakdown of feed-pump pressure (corresponding to Eq. (29)) shows that the most significant component is from the osmotic pressure which increases over the cycle, amplified by the non-ideal correction factors S_P. S_L and S_R – whereas the cross-flow friction term ΔP_m makes negligible contribution to feed pump pressure (Fig. 4). The salt retention is S_R = 1.14 at 80% recovery, compared to S_R = 1.09 reported by Wei et al. in their study of a bladder-type batch RO system at 50% recovery [24]. These values are consistent in the sense that, according to Eq. (26), S_R is expected to increase with recovery. In the optimised design, $SEC_{p,feed}$, $SEC_{p,recir}$, $SEC_{r,feed}$, $SEC_{r,recir}$ and SEC_{aux} contribute respectively 91.64%, 2.98%, 0.12%, 1.23% and 4.03% to total *SEC*.

4.3. Sensitivity analysis

Using the baseline design established above, this section

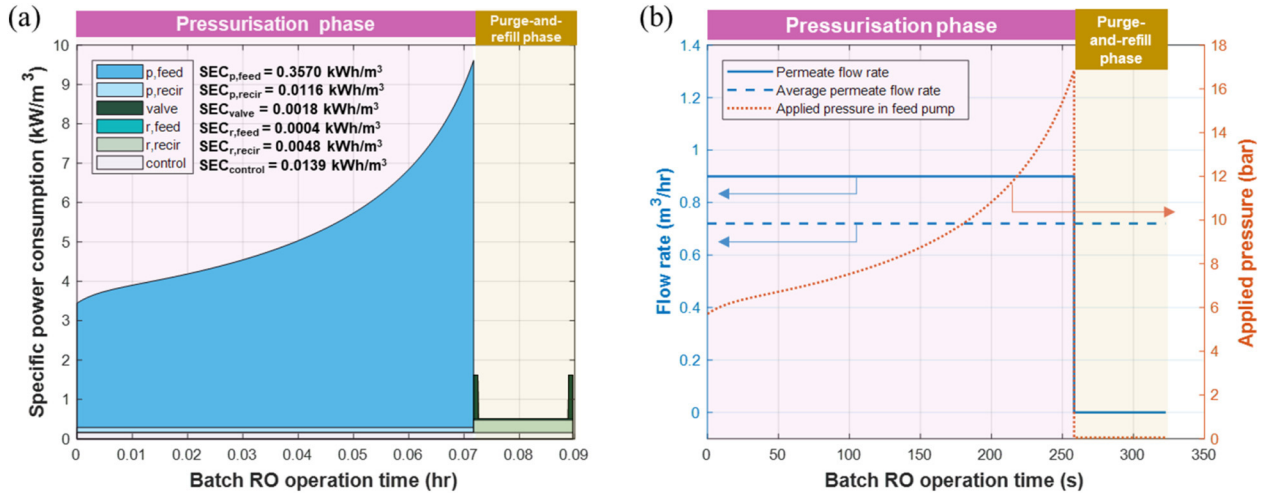

Fig. 3. (a) Specific power consumption, showing each SEC component as an area under the curve; (b) permeate flow and applied pressure over the batch RO cycle (optimised design).

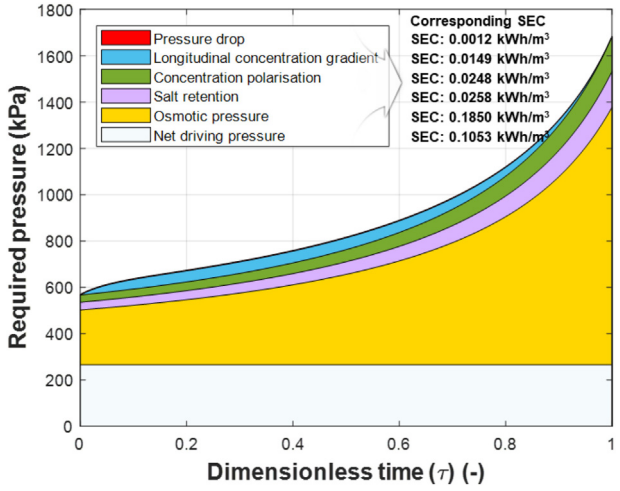

Fig. 4. Detailed analysis of the component $SEC_{p,feed}$ in Fig. 3. Feed pump pressure against dimensionless time ($\tau = t/t_p$) from the cycle start (showing each *SEC* subcomponent as the area beneath the curve).

investigates the effect on performance of varying the design parameters. Parameters have the values of the baseline design expect where stated otherwise. The sensitivity analysis also serves to investigate the influence of assumptions used in the model inputs.

4.3.1. Sensitivity to recovery, recirculation rate and membrane type

As recovery increases above the $r = 0.8$ baseline, *SEC* increases but remains below 0.6 kWh/m^3 at $r = 0.9$ (Fig. 5a). Permeate quality also worsens, as reflected by increased C_{perm}, but C_{perm} remains below 0.25 kg/m^3 (Fig. 5b). The increase in C_{perm} can be offset by increasing α, because recirculation helps to mitigate concentration gradients (S_P and S_L) responsible for driving more salt through the membrane. Changing the membrane type to high-rejection improves the rejection and permeate quality, but at the expense of increased *SEC* (Fig. 5c and d). The average pressure and peak pressure in each case are shown in Fig. S7.

The general pattern of optimisation is similar for the two membranes. For minimum *SEC*, the optimum α increases with r and is generally in the range $2.0 < \alpha < 3.5$. This is consistent with previous findings that the recirculation rate should be 2–3 times the feed flow for efficient batch RO [17]. However, α does not have a strong influence on *SEC*. Therefore, α may in practice be chosen based on other considerations (such as permeate quality or to mitigate fouling) without impacting on *SEC* unduly (Fig. 5).

The optimisation of α results from the trade-off among the different components of *SEC* (Fig. 5e and f). The important trade-off is between energy consumed by each pump during the pressurisation phase. As α increases, feed pump $SEC_{p,feed}$ decreases (because of reduced S_P and S_L) while recirculation pump $SEC_{p,recir}$ increases (because of increased friction losses). Meanwhile, contributions SEC_r and SEC_{aux} are unimportant for the optimisation of α because they are constant and small, contributing less than 5% to total SEC. The optimised α also results in maximise 2nd law efficiency, obtained by comparison of *SEC* against SEC_{ideal} from Eq. (1). The maximum 2nd law efficiency of batch RO is 33.23% with the high-flux membrane, and 24.66% with the high-rejection membrane (Fig. 5e and f). These values compares favourably against existing brackish water desalination systems, generally reported to have 2nd law efficiency of only 10–15% [30].

Though batch RO maintains good performance at high recovery, there is a penalty in the size of the work exchanger vessel. The swept volume V_{b0} increases sharply with r, reaching $V_{b0} = 0.145$ m^3 at $r = 0.9$ (see Fig. 6, which also shows the relationship between r and the r_p, the recovery ratio in the pressurisation phase). For this reason, recovery above about $r = 0.9$ is probably not practical in the current batch RO design, because of the large size and capital cost.

4.3.2. Sensitivity to permeate flux J_w

Low permeate flux J_w is favourable to decrease energy consumption *SEC* through decreased concentration polarisation S_p and lower net driving pressure. The variation of *SEC* with J_w is approximately linear above $J_w = 15$ L/m^2/h, with the main contribution to *SEC* occurring during pressurisation (corresponding to SEC_p in Fig. 7a). At lower fluxes, however, other contributions to *SEC* (such as SEC_{aux}) have a significant influence on the overall *SEC*. Thus, there are diminishing returns from lowering J_w below 15 L/m^2/h. Moreover, too low J_w reduces the output and permeate quality of the batch RO system, since output is directly proportional to J_w. Permeate quality improves up to about $J_w = 25$ L/m^2/h at which point a plateau is reached in the curve of C_{perm} vs. J_w (Fig. 7b).

The high-rejection membrane shows similar results to the high-flux membrane, but with increased energy consumption and the salt rejection (Fig. 7c and d). The salt rejection reaches 98% above $J_w = 15$ L/m^2/h and remains above 96% even at lower permeate flux of $J_w = 10$ L/m^2/h.

Overall, Fig. 7 suggests that J_w should be chosen in the range 10–25 L/m^2/h according to the relative importance of energy

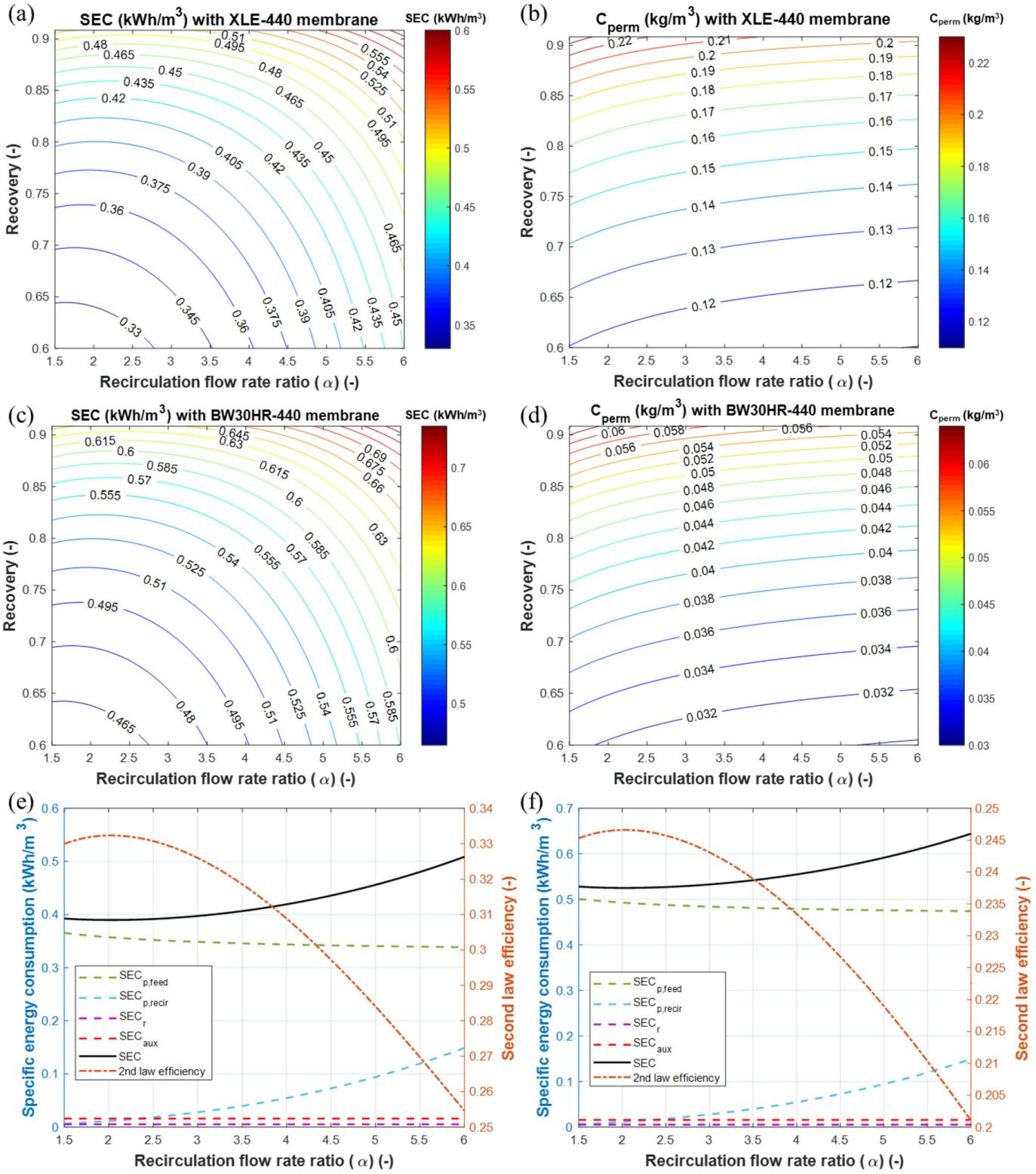

Fig. 5. *SEC* and C_{perm} of the batch RO system depending on the recirculation flow rate α and recovery r. (a) *SEC* and (b) C_{perm} with high-flux (XLE-440) membrane; (c) *SEC* and (d) C_{perm} with high-rejection (BW30HR-440) membrane; SEC breakdown and 2nd law efficiency $r = 0.8$ with (e) high flux membrane and (f) high rejection membrane, showing how the different components sum to determine the optimum α. Lower C_{perm} indicates improved permeate quality.

efficiency, permeate quality and output, and to the membrane type selected. A low permeate flux is favourable to lower *SEC* and running cost, but decrease output thus increasing capital cost.

4.3.3. Sensitivity to water and salt permeabilities

Water and salt permeabilities of the RO membrane can be decreased from the values of virgin membrane during normal operation due to membrane fouling (including organic and inorganic) and scaling [59–62]. So, a sensitivity analysis to water and salt permeabilities

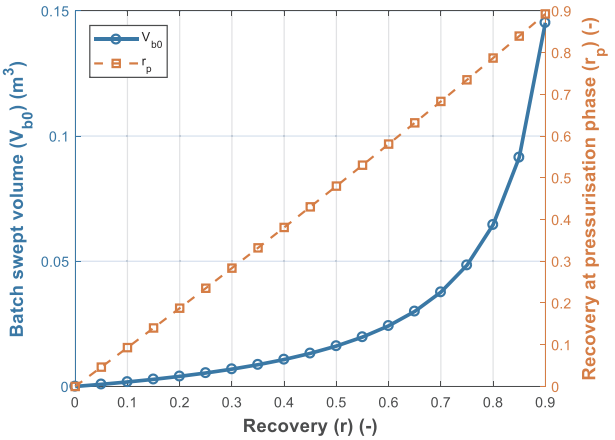

Fig. 6. Correlation between r and V_{b0}, and between r and r_p. Large recovery requires a large swept volume increasing the size of the system substantially.

indicates how much *SEC* and R_s may change when membrane fouling and scaling occur. A pilot-scale RO system showed 30% and 50% decline in water and salt permeability respectively during normal operation over more than 100 days [60]. These reductions may be a good basis to determine ranges of permeabilities in this sensitivity analysis.

As shown in Fig. 8, the decreased water and salt permeabilities increase *SEC* and R_s. The reduced water permeability raises net driving pressure, so this is the main reason for the increased pressure and *SEC*. Meanwhile, the reduced salt permeability enhances the permeate quality with increasing R_s. If water and salt permeabilities are reduced by 30 and 50% respectively ($A = 1.62 \times 10^{-11}$ m/s/Pa and $B = 6.3 \times 10^{-8}$ m/s), in the case of the high-flux membrane, *SEC* increases from 0.3896 kWh/m^3 to 0.4348 kWh/m^3 (11.6% increase as shown in Fig. 8a) and R_s increases from 94.2% to 97.3% (a 3.3% increase as shown in Fig. 8b). In the case of the high-rejection membrane, *SEC* and R_s are correspondingly increased to 0.6284 kWh/m^3 and 99.26% respectively, showing a 19.7% and 0.8% increase over pre-fouled values (Fig. 8c and d). In summary, a penalty of more than 10% is expected in *SEC* under severe fouling and scaling conditions; thus, it is important to control fouling to maintain high energy efficiency in batch RO.

4.3.4. *Sensitivity to pump efficiency*

As shown in Section 4.2, most energy in batch RO is consumed by the feed pump, making feed pump efficiency an important parameter. We investigated sensitivity to the feed pump efficiency on *SEC* and 2nd law efficiency. With the high-flux membrane, *SEC* decreases from 0.3896 kWh/m^3 to 0.2820 kWh/m^3, while 2nd law efficiency increases from 33.23% to 45.93%, if feed pump efficiency increases from 70 to 100% (Fig. 9a). With high-rejection membrane (Fig. 9b), the *SEC* and 2nd law efficiency with 100% feed pump efficiency are 0.3768 kWh/m^3

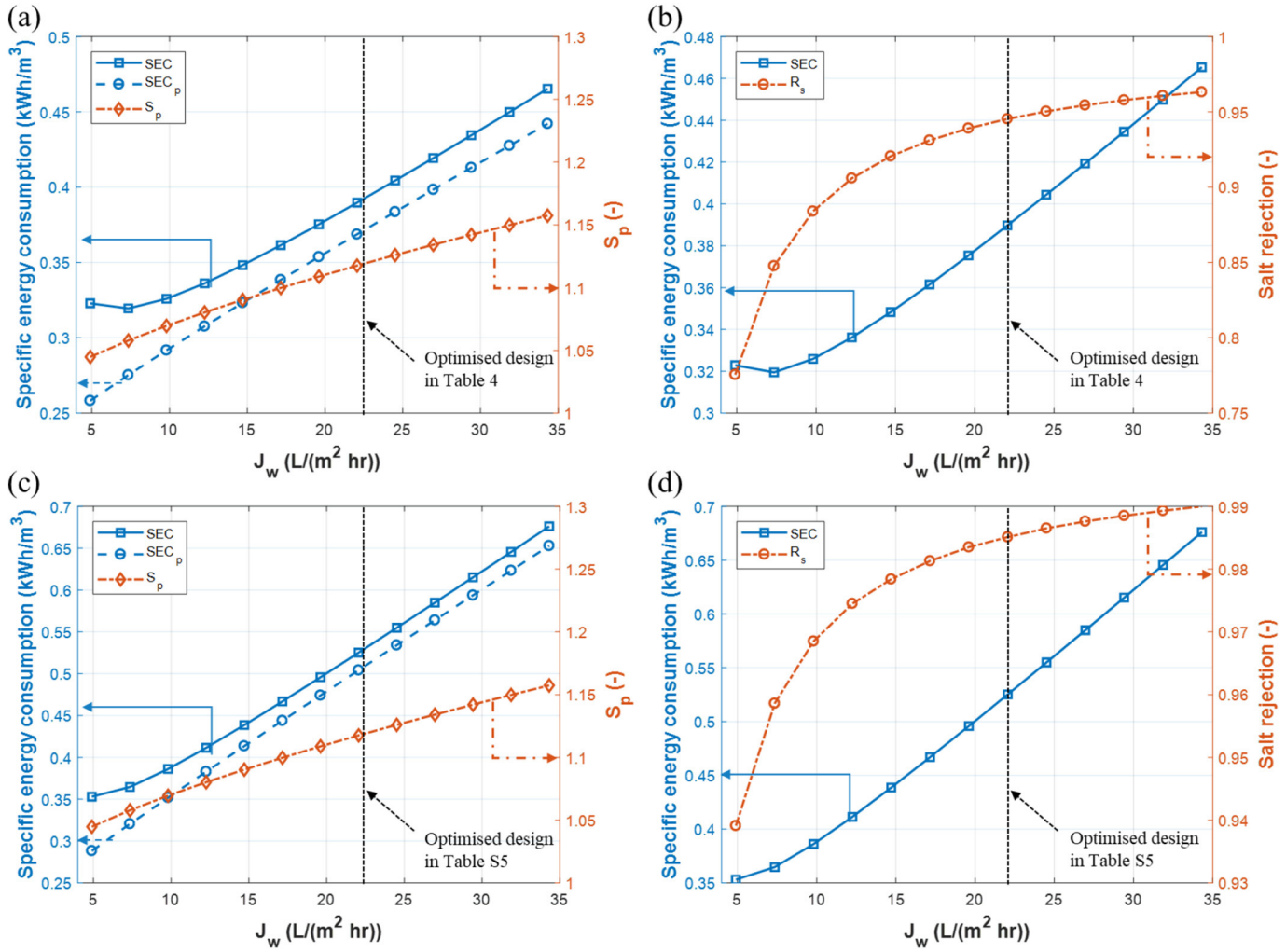

Fig. 7. Sensitivity analysis by changing permeate flux J_w (a) the effect on *SEC* and S_P, (b) the effect on *SEC* and R_s, for high-flux membrane; (c) and (d) similarly for high-rejection membrane.

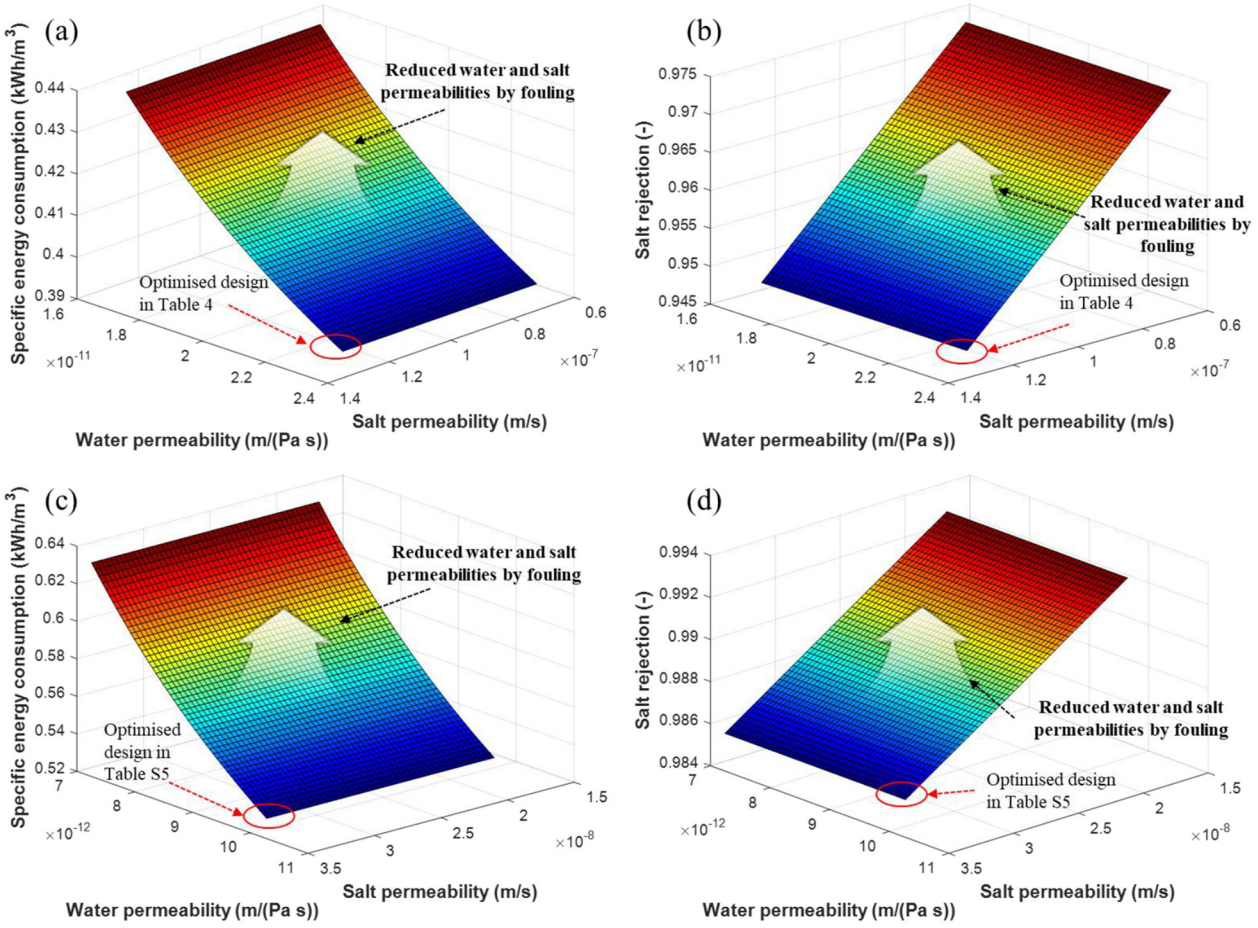

Fig. 8. Sensitivity analysis by changing water permeability A and salt permeability B (a) the effect on SEC, (b) the effect on R_s, for high-flux membrane; (c) and (d) similarly for high-rejection membrane.

and 34.37% respectively. In practice, 100% pump efficiency is unachievable. However, state-of-the-art feed pumps may reach 85% efficiency in larger systems, thus suggesting significant scope for improvement in batch RO [7].

The results in this section reveal the energetic-feasibility of the batch RO for brackish water desalination system with high-recovery. Typically, the SEC of existing brackish water RO is approximately 0.5–1.5 kWh/m^3 [7,63,64]. For example, Qureshi and Zubair [65] calculated SEC = 0.54 kWh/m^3 in conventional brackish water RO using an ERD, at conditions of 3 kg/m^3 feed concentration, 77.5% recovery and 85% pump efficiency – but with no consideration of concentration polarisation. At 77.5% recovery and 85% feed pump efficiency, we predict SEC of batch RO as 0.3150 kWh/m^3 with a high-flux membrane and 0.4266 kWh/m^3 with a high-rejection membrane. Karabelas et al. investigated brackish and seawater RO, reporting SEC = 0.378 kWh/m^3 with brackish water [66]. However, the conditions were 2 kg/m^3 feed concentration, 70% recovery and 85% pump efficiency, so the corresponding 2nd law efficiency was only 19.6%. Many brackish water RO systems do not use any ERD, making their SEC higher. Regarding semi-batch and other batch systems, Stover [47]

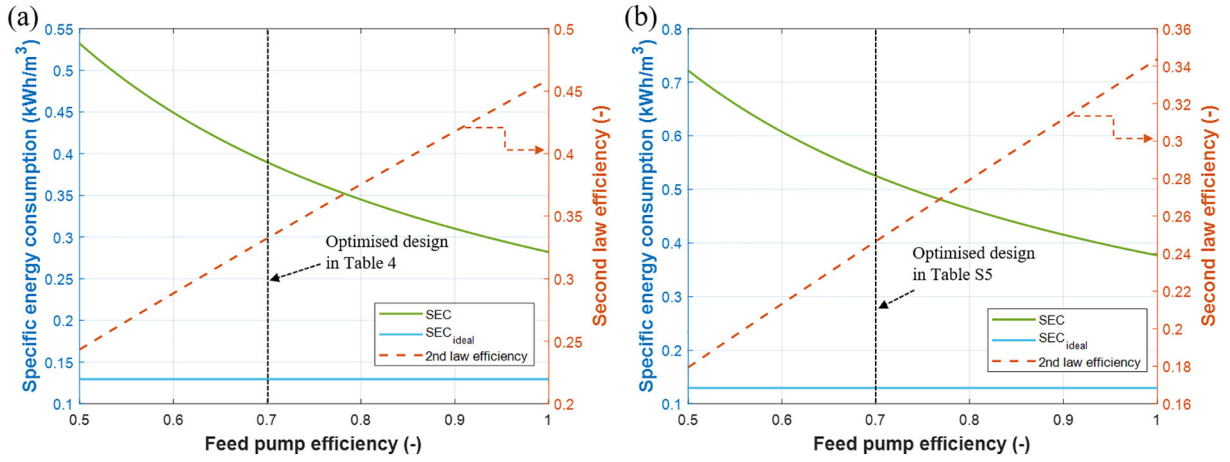

Fig. 9. Sensitivity analysis on SEC and 2nd law efficiency by changing feed pump efficiency (a) for high-flux membrane, and (b) for high-rejection membrane.

compared the actual performance of a semi-batch system to the theoretical performance of conventional brackish water desalination systems operating under the same conditions (fixed recovery of 88% and feedwater containing 2.455 kg/m^3 total dissolved solids). A value of SEC = 0.77 kWh/m^3 was reported for the semi-batch process, whereas SEC = 1.19 kWh/m^3 was calculated for the conventional system running at the same conditions. The batch RO using a free-piston design can produce fresh water from brackish groundwater feed solution (3 kg/m^3 of concentration) with low-energy consumption (about 0.4 kWh/m^3) and 2nd law efficiency of 33.2% – substantially higher than conventional brackish water RO which is typically in the range 10–15% [30].

So far relatively few comparative results are available for batch systems. Wei et al. tested a bladder batch RO system and reported SEC of < 0.32 kWh/m^3 when operated with feed water concentration of 2–5 kg/m^3 [23]. However, this system was limited to an operating pressure of 10 bar and recovery of 55%. Further, the SEC calculation was based on hydraulic rather than electrical work i.e. assuming pump efficiency of 100%. Introducing a pump efficiency of 70% would raise SEC to < 0.46 kWh/m^3 which is comparable to the prediction of the current study. In summary, batch RO is a promising method for low-energy desalination of brackish water at high-recovery.

5. Conclusions

We have designed a free-piston batch RO system and modelled its performance using two types of 8-inch spiral wound membrane: a high-flux and a high-rejection type. The system operates cyclically in two phases (pressurisation then purge-and-refill) using two pumps (a feed pump and a recirculation pump) and three on-off valves. A detailed design procedure has been developed using only algebraic equations, making it straightforward to apply. A system has been designed and optimised for brackish water feed at concentration 3 kg/m^3 NaCl.

- At recovery r = 0.8, the optimised design with high-flux membrane results in SEC = 0.39 kWh/m^3, a total output of 17.3 m^3/day and rejection of 94.2%; whereas with the high-rejection membrane, SEC rises to 0.525 kWh/m^3 but rejection improves to 98.5%.
- This SEC of 0.39 kWh/m^3 corresponds to 2nd law efficiency of 33.2%, thus comparing well to existing brackish water desalination systems that typically have SEC in the range 0.5–1 kWh/m^3 and second law efficiency of only 10–15% [30].
- Non-ideal correction factors (concentration polarisation, longitudinal concentration gradient, and salt retention) have been included, as well as membrane pore friction, and friction losses in the RO module and pipework.
- Sensitivity to recovery, recirculation flow rate, membrane type, permeate flux, membrane permeabilities, and pump efficiency was investigated, showing the applicability of the batch RO in cases of high recovery, high rejection, and high fouling propensity.

The study has highlighted that the free-piston batch-RO is an efficient solution for brackish water desalination at high recovery (up to about 0.9) with outputs up to about 20 m^3/day using a single 8-inch RO module. It may be extended to other configurations of batch RO desalination using free pistons, including multi-module versions for increased output. The batch RO system contrasts with most existing RO systems in that it uses unsteady conditions. There are many opportunities for future research to explore in more depth how the unsteady conditions will influence behaviour including long-term efficiency and fouling resistance.

Nomenclature

Roman and Greek symbols

A	m/(s·Pa), Water permeability
A_m	m^2, Membrane area
B	m/s, Salt permeability
C	kg/m^3, Concentration
D	m^2/s, Diffusivity
d_{pipe}	m, Pipe diameter
E	kJ (kWh), Energy consumption
f	–, Friction factor
G	–, Coefficient in Eq. (24)
H	m, Membrane channel height
J_w	m/s (l/m^2/h), Permeate flux
J_s	kg/(m^2/s), Salt flux
K_i	–, Loss coefficient of i'th fitting
K_1, K_∞, K_d	–, Coefficients of 3-K method for estimation of pressure drop
k	m/s, Mass transfer coefficient
L	m, Length
n	–, Coefficient in Eq. (24)
P	kPa (bar), Pressure
$\overline{P}$	kPa (bar), Volume-weighted average pressure
$\widehat{P}$	kPa (bar), Peak pressure
Q	m^3/s, Flow rate
$\overline{Q}$	m^3/s, Average flow rate
Re	–, Reynolds number
R_s	–, Salt rejection
r	–, Recovery
r_p	–, Recovery at pressurisation phase
Sc	–, Schmidt number
Sh	–, Sherwood number
S_L	–, Longitudinal concentration gradient factor
S_P	–, Concentration polarisation factor
S_R	–, Salt retention factor
t	s, Time
V	m^3, Volume
V_{b0}	m^3, Batch swept volume
V_{pipe}	m^3, Pipe volume
V_{pg}	m^3, Purged volume
$V_{pipe,R}$	m^3, Retained solution volume in pipes
v	m/s, Velocity
W_{actual}	kWh, Actual work
W_{ideal}	kWh, Ideal work
w	m, Membrane width
α	–, Ratio of recirculation flow rate to the permeate (or feed) flow rate
γ	–, Dimensionless concentration
λ	–, Longitudinal dispersion factor in the RO module
ΔP	kPa, Pressure drop
η	–, Pump efficiency
μ	Pa·s, Viscosity
π	kPa, Osmotic pressure
ρ	kg/m^3, Density
τ	–, Dimensionless time

Superscripts and subscripts

0	Initial state of batch RO cycle
aux	Auxiliary
b	Batch
brine	Concentrated brine
ctr	Controller
cycle	Single batch-RO cycle
feed	Feed stream

i	Referring to *i*'th fitting
ideal	Ideal state
in	Inlet stream to the RO module
m	Membrane
out	Outlet stream from the RO module
p	Pressurisation phase
perm	Permeate stream
pg	Purge region
pipe	Pipe
ports	Ports of RO membrane
r	Purge-and-refill phase
R	Retained region
recir	Recirculation stream
valves	Control valves

Abbreviations

ERD	Energy recovery device
ODE	Ordinary differential equation
PDE	Partial differential equation
PX	Pressure exchanger
RO	Reverse osmosis
SEC	Specific energy consumption
SWM	Spiral wound module

Author statement

Kiho Park: Conceptualization, Methodology, Formal Analysis, Original Draft, Review and Editing.

Liam Burlace: Investigation, Writing, Review and Editing.

Nirajan Dhakal: Conceptualization, Investigation, Writing, Review and Editing.

Anurag Mudgal: Investigation, Writing, Review and Editing.

Neil A. Stewart: Supervision, Review and Editing.

Philip A. Davies: Conceptualization, Validation, Review and Editing, Supervision, Resources.

Declaration of competing interest

The authors declare that they have no known competing financial interests or personal relationships that could have appeared to influence the work reported in this paper.

Acknowledgements

This project has received funding from the European Union's Horizon 2020 research and innovation programme under grant agreement No. 820906 and the Department of Biotechnology (Government of India, Project No. BT/IN/EU-WR/40/AM/2018). LB acknowledges support from the Douglas Bomford Trust. The authors thank Prasanta Dey for his helpful comments on the manuscript.

Appendix A. Modelling the effect of recirculation flow on efficiency of batch RO

In a standard RO system, there is a significant increase in concentration from inlet to outlet. This is avoided in the batch system by using a large recirculation flow. If, however, the recirculation flow is too large, the power consumption of the recirculation pump will outweigh the benefit of recirculation. It is therefore very important to have a methodology to determine the optimum recirculation flow rate for energy minimisation of the batch RO system.

As shown in Fig. A1, the recirculation flow rate influences on the concentration difference between the inlet and outlet streams in the RO module. To describe the correlation between α and $C_{pipe,out}$, mathematical models based on mass balance equations should be derived. In the ideal case of high recirculation flow, the concentration will increase in inverse proportion to the volume remaining in the system. Defining the initial batch swept volume as V_{b0}, the module volume as V_m, the pipe volume as V_{pipe}, and the dead volume in the vessel port as V_{ports}, the volume of the batch vessel at time t can be expressed as;

$$V_b = (1 - \tau)V_{b0} \tag{A1}$$

where, τ is the dimensionless time, that is the time elapsed as fraction of the pressurisation phase duration ($0 < \tau < 1$).

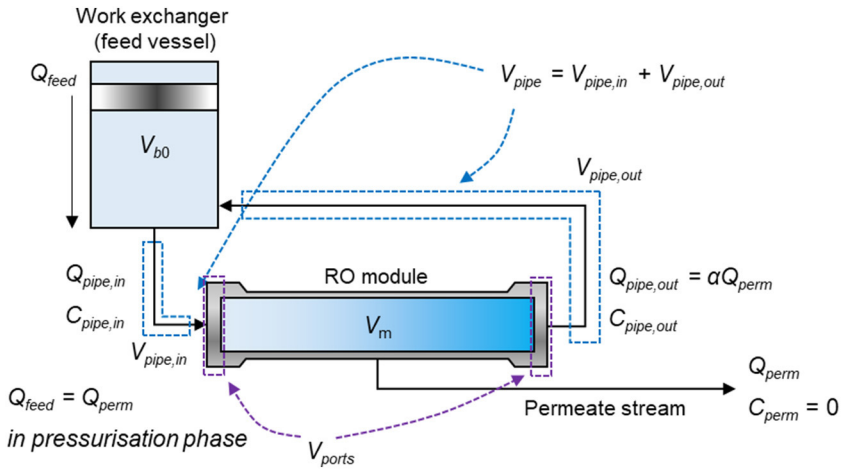

Fig. A1. Schematic diagram of the effect of recirculation flow rate on the concentration difference of inlet and outlet streams in the RO module. V is the volume, Q is the volumetric flow rate, α is the ratio of recirculation flow rate on the permeate flow rate, and C is the concentration.

There are two cases of the concentration difference in the RO module; (1) ideal case where there is negligible concentration increase between inlet and outlet of the RO module, corresponding to nearly infinite recirculation flow, and (2) actual case where the concentration difference is affected by the recirculation flow rate. By comparing these cases, the deviation in the actual system from the ideal case can be evaluated.

(1) Ideal case (infinite recirculation rate)

In the ideal case, the volume fraction can be expressed by rearranging the Eq. (A1).

$$\frac{V_b}{V_{b0} + V_m + V_{pipe} + V_{ports}} = 1 - r_p\tau \tag{A2}$$

where, r_p is the recovery ratio in the pressurisation phase which can be expressed as $r_p = V_{b0}/V_0 = V_{b0}/(V_{b0} + V_m + V_{pipe} + V_{ports})$. If the permeate stream could be assumed as zero concentration (no salt permeation through the RO membrane), the amount of salt in the initial batch volume is consistently retained in the volume at time t. As the initial batch concentration is C_0, the concentration ratio (γ) of C at time t over C_0 can be expressed as:

$$C \bullet V_b = C_0(V_{b0} + V_m + V_{pipe} + V_{ports}) \tag{A3}$$

$$\gamma = \frac{C}{C_0} = \frac{1}{1 - r_p\tau} \tag{A4}$$

With an assumption that the osmotic pressure in the batch system is proportional to the concentration, the ideal work in the batch RO system (W_{ideal}) is given as:

$$W_{ideal} = \int_0^{V_{b0}} -PdV_b = \pi_0 V_{b0} \int_0^1 \gamma d\tau = \pi_0 V_{b0} \frac{1}{r_p} \ln \frac{1}{1 - r_p} \tag{A5}$$

where, P is the pressure, and π_0 is the osmotic pressure of C_0. This gives Eq. (1).

(2) Actual case (finite recirculation rate)

To estimate the required work in the actual system, we follow the assumptions of constant density and the van't Hoff law (osmotic pressure proportional to concentration). We also assume that the RO membrane has 100% rejection, so the concentration of permeate stream is zero. We assume that the concentration in the feed vessel is well-mixed.

It is also assumed that the concentration in the RO element varies linearly from inlet to outlet, such that the mass of salt in the module may be estimated as the average of inlet and outlet concentrations: mass salt $= 0.5 \times V_m(C_{pipe,in} + C_{pipe,out})$. Pressure and work needed is proportional to the average concentration in the RO module.

We estimate the effect of the recirculation flow rate by seeing its impact on $C_{pipe,out}$ compared to the ideal case given by Eq. (A4). We integrate $C_{pipe,out}$ over the cycle and compare it to Eq. (A5) to the see the penalty in SEC, as a fraction of ideal SEC, due to non-infinite recirculation flow rate. This approach follows from the initial rationale of the batch-RO design which is to minimise osmotic pressure at module outlet.

Just two equations are used to calculate the inlet and outlet concentrations $C_{pipe,in}$ and $C_{pipe,out}$ (expressed in dimensionless form as ratios to initial feed concentration C_0 filling the system, i.e. $\gamma_{pipe,in} = C_{pipe,in}/C_0$ and $\gamma_{pipe,out} = C_{pipe,out}/C_0$). The first is a differential equation for mass balance in the batch vessel, as its volume decreases with time:

$$(1 - \tau)\frac{d\gamma_{pipe,in}}{d\tau} = \alpha(\gamma_{pipe,out} - \gamma_{pipe,in}) \tag{A6}$$

where, α is the recirculation flow ratio, which is defined as the outlet flow rate over the permeate flow rate as shown in Fig. A1.

The second is a mass conservation considering that the overall mass must remain constant (assumption of no salt escapes):

$$\gamma_{pipe,out} - \gamma_{pipe,in} = \frac{2}{1 - r_p}[1 - \gamma_{pipe,in}(1 - r_p\tau)] \tag{A7}$$

The detailed derivations of the Eqs. (A6) and (A7) are given in Appendix B. Substituting Eqs. (A7) in (A6), the equation can be arranged as:

$$(1 - \tau)\frac{d\gamma_{pipe,in}}{d\tau} = \frac{2\alpha}{1 - r_p}[1 - \gamma_{pipe,in}(1 - r_p\tau)] \tag{A8}$$

By solving the Eqs. (A7) and (A8), $\gamma_{pipe,in}$ and $\gamma_{pipe,out}$ can be calculated. In this study, the solution of Eq. (A8) was obtained by a differential equation solver (default setting of ode45 in MATLAB 2019b). The actual work in the batch RO system can be calculated by applying the Eq. (A5), but the equation was changed to consider the effect of concentration difference inside the RO module as follows:

$$W_{actual} = \int_0^{V_{b0}} -PdV_b = \pi_0 V_{b0} \int \left(\frac{\gamma_{pipe,in} + \gamma_{pipe,out}}{2}\right) d\tau \tag{A9}$$

The integration is conducted by the trapezoidal rule. By comparing the Eqs. (A5) and (A9), the deviation of the actual work from the ideal work can be estimated. In the ideal case, there is no concentration rise along the RO module. On the other hand, the outlet concentration ($C_{pipe,out}$) is always higher than the inlet concentration ($C_{pipe,in}$) in the actual case because of the permeate flux. Therefore, the ratio of W_{actual}/W_{ideal} describes the energy-inefficiency in the module-scale operation.

$$S_L = \frac{W_{actual}}{W_{ideal}} = \frac{\int \left(\frac{\gamma_{pipe,in} + \gamma_{pipe,out}}{2}\right) d\tau}{\int \gamma d\tau} \tag{A10}$$

Following the numerical solution to the above, we developed an empirical equation as shown in Eq. (24) to avoid the utilisation of the numerical methods so that the simulation of batch RO can be easily executed. The estimated coefficients of Eq. (24) are listed in Table 2 and further details of their fit and accuracy are given in the SI.

Appendix B. Derivation of mass balance equations in the batch RO system

In the feed vessel displayed in Fig. A1, the mass balance equation can be formulated by setting the batch volume variable at time t as V_b:

$$\frac{d(V_b C_{pipe,in})}{dt} = Q_{pipe,out} C_{pipe,out} - Q_{pipe,in} C_{pipe,in} \tag{B1}$$

By applying chain rule, the Eq. (B1) can be arranged as:

$$C_{pipe,in} \frac{dV_b}{dt} + V_b \frac{dC_{pipe,in}}{dt} = Q_{pipe,out} C_{pipe,out} - Q_{pipe,in} C_{pipe,in} \tag{B2}$$

If it is assumed that constant density is maintained in the whole system (due to low concentration), the volume change in the feed vessel can be expressed as:

$$V_b = V_{b0} - Q_{feed} t \tag{B3}$$

$$Q_{feed} = -\frac{dV_b}{dt} \tag{B4}$$

From the definition in Fig. A1 and volume balance with the assumption of constant density, $Q_{pipe,in}$ and $Q_{pipe,out}$ can be expressed as:

$$Q_{pipe,out} = \alpha Q_{feed} \tag{B5}$$

$$Q_{pipe,in} = (\alpha + 1) Q_{feed} \tag{B6}$$

By substituting Eqs. (B3)–(B6) into Eq. (B2), the Eq. (B2) can be rearranges in terms of Q_{feed} as follows:

$$- C_{pipe,in} Q_{feed} + (V_{b0} - Q_{feed} t) \frac{dC_{pipe,in}}{dt} = \alpha Q_{feed} C_{pipe,out} - (\alpha + 1) Q_{feed} C_{pipe,in} \tag{B7}$$

Dividing both side of Eq. (B7) by Q_{feed} and C_0, the Eq. (B7) can be changed to dimensionless form.

$$- \gamma_{pipe,in} + (t_p - t) \frac{d\gamma_{pipe,in}}{dt} = \alpha \gamma_{pipe,out} - (\alpha + 1) \gamma_{pipe,in} \tag{B8}$$

where, t_p is the elapsed time in the pressurisation phase in each batch RO cycle, which can be defined as V_{b0}/Q_{feed}. To make the Eq. (B8) dimensionless form completely, the time variable was changed by dividing T as follows:

$$(1 - \tau) \frac{d\gamma_{pipe,in}}{d\tau} = \alpha (\gamma_{pipe,out} - \gamma_{pipe,in}) \tag{B9}$$

where, τ is the dimensionless time, which is defined as t/t_p and the same to Eq. (A1). Therefore, Eq. (B9) can be derived and applied in Eq. (A6) in Appendix A.

To derive the Eq. (A7), overall mass balance equation in the whole batch RO system is formulated as follows:

$$(V_{b0} + V_m + V_{pipe} + V_{ports}) C_0 = (V_{b0} - Q_{feed} t) C_{pipe,in} + \frac{V_m + V_{pipe} + V_{ports}}{2} (c_{pipe,in} + c_{pipe,out}) \tag{B10}$$

In Eq. (B10), the left-hand side term denotes initial mass of salt in the batch RO system, and the first and second terms in the right-hand side denote the amount of mass retained in the feed vessel at time t and the amount of mass in the RO module and pipes at time t, respectively. Although $V_{pipe,in}$ and $V_{pipe,out}$ are usually slightly different, these volumes are assumed equal to avoid complexity in solving Eq. (B10). This is a reasonable assumption, because V_{pipe} is much smaller than V_m, so the exact assumption made about the pipe volumes is not too important. (Neglecting the pipe volumes would give the same result as considering them equal). These simplifying assumptions allow a general formula to be derived for S_L. By using the definition of r_p, $\gamma_{pipe,in}$, and $\gamma_{pipe,out}$ in Appendix A, Eq. (B10) can be arranged as:

$$\frac{V_{b0}}{r_p} = V_{b0} (1 - \tau) \gamma_{pipe,in} + \frac{V_{b0} (1 - r_p)}{2 r_p} (\gamma_{pipe,in} + \gamma_{pipe,out}) \tag{B11}$$

$$\gamma_{pipe,in} + \gamma_{pipe,out} = \frac{2[1 - r_p (1 - \tau) \gamma_{pipe,in}]}{1 - r_p} \tag{B12}$$

$$\gamma_{pipe,out} - \gamma_{pipe,in} = \frac{2[1 - r_p (1 - \tau) \gamma_{pipe,in}]}{1 - r_p} - 2\gamma_{pipe,in} \tag{B13}$$

$$\gamma_{pipe,out} - \gamma_{pipe,in} = \frac{2[1 - \gamma_{pipe,in} (1 - r_p \tau)]}{1 - r_p} \tag{B14}$$

Thus, the Eq. (A7) in Appendix A can be obtained from the overall mass balance.

Appendix C. Modelling of the effect of salt retention in each batch RO cycle

After the water production in the pressurisation phase, the concentrated brine should be purged, and a new feed solution is supplied to restart the batch RO cycle. However, some of the volume cannot be refilled by the new feed solution, which causes a salt retention effect in each batch RO cycle [24]. As shown in Fig. 1b, the volume of the RO module itself and the pipes connected to the RO module can be purged and refilled, while the volume of pipes connected to recirculation pump and between the work exchanger and the RO module cannot be purged. The retained salt increases the

concentration at the start of the next cycle, which increases the required SEC for water treatment. Therefore, this salt retention factor should be carefully considered for estimation of the SEC in the batch RO system.

The overall volume inside the batch RO system can be categorised as three groups, purge volume (V_{pg}), batch swept volume (V_{b0}), and retained pipe volume ($V_{pipe,R}$), as shown in Fig. 1b. The purge volume (including pipes, RO membrane module, and dead volume in the vessel ports, which is a summation of $V_{pipe,pg}$, V_m, and V_{ports}) is the brine solution volume that can be replaced by the new feed solution at the purge-and-refill phase. The batch swept volume (inside the work exchanger) is the permeate volume in the pressurisation phase. In other words, the batch swept volume is the difference between the initial volume and the final volume in the pressurisation phase. Finally, the retained pipe volume is the remaining volume of concentrated brine after the purge-and-refill phase. The summation of these three volumes is the initial volume at each batch RO cycle as follows:

$$V_0 = V_{pg} + V_{b0} + V_{pipe,R} \tag{C1}$$

The effect of salt retention in the retained pipe volume on the overall energy consumption can be derived from mass balance equations. With assumptions that the batch RO system reaches its steady-state, which means there is no concentration difference at the initial concentrations of each RO cycle, and there is no salt permeation through the RO membrane, the amount of mass fed into the batch RO system before the pressurisation phase is the same to the amount of mass rejected from the batch RO system in the purge-and-refill phase as follows:

$$(V_{b0} + V_{pg})C_{feed} = V_{pg}C_{feed} + (C_{brine} - C_{feed})(1 - \lambda)V_{pg} \tag{C2}$$

where, C_{brine} is the concentration of the brine at the final of the pressurisation phase. The left-hand side in Eq. (C2) denotes the inlet mass of salt in a single batch RO cycle, and the right-hand side means the outlet mass of salt during the purge-and-refill phase. Because it is assumed that the operation of batch RO cycle has reached in a steady-state, the inlet and outlet mass should be the same.

As reported in our previous study, a longitudinal dispersion in the RO module causes an undesirable mixing due to diffusion and convection in the feed flow at the purge-and-refill phase [15]. The mixing effect increases the concentration of the refilled feed solution higher than the original feed solution. The effect should be considered in the salt retention modelling in the Eq. (C2) as a form of λ. The Eq. (C2) can be rearranged as follows:

$$\frac{C_{brine}}{C_{feed}} = \frac{V_{b0}}{(1 - \lambda)V_{pg}} + 1 \tag{C3}$$

Because the actual recovery ratio in the batch RO system (r) was defined as $V_{b0}/(V_{b0} + V_{pg})$, the Eq. (C3) can be arranged with r as follows:

$$\frac{C_{brine}}{C_{feed}} = \frac{r}{(1 - \lambda)(1 - r)} + 1 \tag{C4}$$

At the beginning of the pressurisation phase, the initial batch concentration (C_0) in each cycle at steady-state can be calculated by the mass balance equation as follows:

$$C_0 V_0 = (V_{pg} + V_{pipe,R})C_{brine} \tag{C5}$$

The left-hand side of the Eq. (C5) is the amount of salt at the beginning of the pressurisation phase, and the right-hand is the amount of salt after the pressurisation phase. The Eq. (C5) can be arranged as:

$$\frac{C_0}{C_{brine}} = \frac{V_{pg} + V_{pipe,R}}{V_{b0} + V_{pg} + V_{pipe,R}} = \frac{(1 - r)\left(1 + \frac{V_{pipe,R}}{V_{pg}}\right)}{1 + (1 - r)\frac{V_{pipe,R}}{V_{pg}}} \tag{C6}$$

The salt retention ratio (S_R) is defined as C_0/C_{feed}, which can be obtained by incorporating the Eqs. (C4) and (C6) as follows:

$$S_R = \frac{C_0}{C_{feed}} = \frac{C_0}{C_{brine}}\frac{C_{brine}}{C_{feed}} = \frac{(1 - r)\left(1 + \frac{V_{pipe,R}}{V_{pg}}\right)}{1 + (1 - r)\frac{V_{pipe,R}}{V_{pg}}}\left[\frac{r}{(1 - \lambda)(1 - r)} + 1\right] \tag{C7}$$

$$S_R = \frac{\left(1 + \frac{V_{pipe,R}}{V_{pg}}\right)}{1 + (1 - r)\frac{V_{pipe,R}}{V_{pg}}}\left[1 + \frac{r \bullet \lambda}{(1 - \lambda)}\right] \tag{C8}$$

Appendix D. Supplementary data

Supplementary data to this article can be found online at https://doi.org/10.1016/j.desal.2020.114625.

References

[1] M. Elimelech, W.A. Phillip, The future of seawater desalination: energy, technology, and the environment, Science 333 (2011) 712–717.

[2] A.D. Khawaji, I.K. Kutubkhanah, J.-M. Wie, Advances in seawater desalination technologies, Desalination 221 (2008) 47–69.

[3] J. Kim, K. Park, D.R. Yang, S. Hong, A comprehensive review of energy consumption of seawater reverse osmosis desalination plants, Appl. Energy 254 (2019) 113652.

[4] K. Park, J. Kim, D.R. Yang, S. Hong, Towards a low-energy seawater reverse osmosis desalination plant: a review and theoretical analysis for future directions, J. Membr. Sci. 595 (2020) 117607.

[5] U. Caldera, C. Breyer, Assessing the potential for renewable energy powered desalination for the global irrigation sector, Sci. Total Environ. 694 (2019) 133598.

[6] K. Park, D.Y. Kim, Y.H. Jang, M.-g. Kim, D.R. Yang, S. Hong, Comprehensive analysis of a hybrid FO/crystallization/RO process for improving its economic feasibility to seawater desalination, Water Res. 171 (2020) 115426.

[7] N. Voutchkov, Energy use for membrane seawater desalination–current status and trends, Desalination 431 (2018) 2–14.

[8] S. Kim, D. Cho, M.-S. Lee, B.S. Oh, J.H. Kim, I.S. Kim, SEAHERO R&D program and key strategies for the scale-up of a seawater reverse osmosis (SWRO) system, Desalination 238 (2009) 1–9.

[9] A. Villafafila, I. Mujtaba, Fresh water by reverse osmosis based desalination: simulation and optimisation, Desalination 155 (2003) 1–13.

[10] J. Kim, D.I. Kim, S. Hong, Analysis of an osmotically-enhanced dewatering process for the treatment of highly saline (waste) waters, J. Membr. Sci. 548 (2018) 685–693.

[11] A. Shrivastava, S. Rosenberg, M. Peery, Energy efficiency breakdown of reverse osmosis and its implications on future innovation roadmap for desalination, Desalination 368 (2015) 181–192.
[12] D.M. Warsinger, E.W. Tow, K.G. Nayar, L.A. Maswadeh, J.H. Lienhard V, Energy efficiency of batch and semi-batch (CCRO) reverse osmosis desalination, Water Res. 106 (2016) 272–282.
[13] J.R. Werber, A. Deshmukh, M. Elimelech, Can batch or semi-batch processes save energy in reverse-osmosis desalination? Desalination 402 (2017) 109–122.
[14] M. Barello, D. Manca, R. Patel, I.M. Mujtaba, Operation and modeling of RO desalination process in batch mode, Comput. Chem. Eng. 83 (2015) 139–156.
[15] T. Qiu, P.A. Davies, Longitudinal dispersion in spiral wound RO modules and its effect on the performance of batch mode RO operations, Desalination 288 (2012) 1–7.
[16] T. Qiu, P.A. Davies, Comparison of configurations for high-recovery inland desalination systems, Water 4 (2012) 690–706.
[17] T. Qiu, P. Davies, Concentration polarization model of spiral-wound membrane modules with application to batch-mode RO desalination of brackish water, Desalination 368 (2015) 36–47.
[18] P.A. Davies, J. Wayman, C. Alatta, K. Nguyen, J. Orfi, A desalination system with efficiency approaching the theoretical limits, Desalin. Water Treat. 57 (2016) 23206–23216.
[19] E. Jones, M. Qadir, M.T. van Vliet, V. Smakhtin, S.-m. Kang, The state of desalination and brine production: a global outlook, Sci. Total Environ. 657 (2019) 1343–1356.
[20] J. Kim, K. Park, S. Hong, Optimization of two-stage seawater reverse osmosis membrane processes with practical design aspects for improving energy efficiency, J. Membr. Sci. 601 (2020) 117889.
[21] Y. Oren, E. Korngold, N. Daltrophe, R. Messalem, Y. Volkman, L. Aronov, M. Weismann, N. Bouriakov, P. Glueckstern, J. Gilron, Pilot studies on high recovery BWRO-EDR for near zero liquid discharge approach, Desalination 261 (2010) 321–330.
[22] Q.J. Wei, C.I. Tucker, P.J. Wu, A.M. Trueworthy, E.W. Tow, J.H. Lienhard V, Batch reverse osmosis: experimental results, model validation, and design implications, 2019 AMTA/AWWA Membrane Technology Conference & Exposition, American Membrane Technology Association, New Orleans, Louisiana, 2019.
[23] Q.J. Wei, C.I. Tucker, P.J. Wu, A.M. Trueworthy, E.W. Tow, J.H. Lienhard V, True batch reverse osmosis prototype: model validation and energy savings, in: The International Desalination Association World Congress on Desalination and Water Reuse 2019, International Desalination Association, Dubai, UAE, 2019.
[24] Q.J. Wei, C.I. Tucker, P.J. Wu, A.M. Trueworthy, E.W. Tow, J.H. Lienhard V, Impact of salt retention on true batch reverse osmosis energy consumption: Experiments and model validation, Desalination 479 (2020) 114177.
[25] L. Szucz, A. Szucs, Method and apparatus for treating fluids containing foreign materials by membrane filter equipment, US Patent, 4983301 (1991).
[26] H. Abu Ali, M. Baronian, L. Burlace, P.A. Davies, S. Halasah, M. Hind, A. Hossain, C. Lipchin, A. Majali, M. Mark, Off-grid desalination for irrigation in the Jordan Valley, Desalin. Water Treat. 168 (2019) 143–154.
[27] M.J. Staniforth, Performance Analysis and Optimisation of a Saline Groundwater Batch Reverse Osmosis Desalination System for Irrigation and Education in the Jordan Valley, MEng dissertation Aston University, 2018.
[28] J. Swaminathan, E.W. Tow, R.L. Stover, Practical aspects of batch RO design for energy-efficient seawater desalination, Desalination 470 (2019) 114097.
[29] C. Liu, K. Rainwater, L. Song, Energy analysis and efficiency assessment of reverse osmosis desalination process, Desalination 276 (2011) 352–358.
[30] J.H. Lienhard, G.P. Thiel, D.M. Warsinger, L.D. Banchik, Low Carbon Desalination: Status and Research, Development, and Demonstration Needs, Report of a Workshop Conducted at the Massachusetts Institute of Technology in Association with the Global Clean Water Desalination Alliance, (2016).
[31] T. Qiu, Desalination of Brackish Water by a Batch Reverse Osmosis Desalink System for Use With Solar Thermal Energy, PhD Thesis, Aston University (2014).
[32] J. Wayman, Brackish Ground Water Desalination Using Solar Reverse Osmosis, MEng dissertation Aston University, 2015.
[33] P.A. Davies, A solar-powered reverse osmosis system for high recovery of freshwater from saline groundwater, Desalination 271 (2011) 72–79.
[34] O. Igobo, Low-temperature Isothermal Rankine Cycle for Desalination, PhD Thesis, Aston University (2016).
[35] P. Davies, A. Afifi, F. Khatoon, G. Kuldip, S. Javed, S. Khan, Double-acting batch-RO system for desalination of brackish water with high efficiency and high recovery, in: Desalination for the Environment–Clean Energy and Water, Rome, 2016, pp. 23–25.
[36] X. Wang, E. Duitsman, N. Rajagopalan, V. Namboodiri, Chemical treatment of commercial reverse osmosis membranes for use in FO, Desalination 319 (2013) 66–72.
[37] S. Lin, M. Elimelech, Staged reverse osmosis operation: configurations, energy efficiency, and application potential, Desalination 366 (2015) 9–14.
[38] N.M. Mazlan, D. Peshev, A.G. Livingston, Energy consumption for desalination—a comparison of forward osmosis with reverse osmosis, and the potential for perfect membranes, Desalination 377 (2016) 138–151.
[39] J. Sahu, V.A. Juvekar, Development of a rationale for decoupling osmotic coefficient of electrolytes into electrostatic and nonelectrostatic contributions, Fluid Phase Equilib. 460 (2018) 57–68.
[40] C. Bartels, R. Franks, S. Rybar, M. Schierach, M. Wilf, The effect of feed ionic strength on salt passage through reverse osmosis membranes, Desalination 184 (2005) 185–195.
[41] A. Sagiv, N. Avraham, C.G. Dosoretz, R. Semiat, Osmotic backwash mechanism of reverse osmosis membranes, J. Membr. Sci. 322 (2008) 225–233.
[42] W. Zhou, L. Song, T.K. Guan, A numerical study on concentration polarization and system performance of spiral wound RO membrane modules, J. Membr. Sci. 271 (2006) 38–46.
[43] D.M. Warsinger, E.W. Tow, L.A. Maswadeh, G.B. Connors, J. Swaminathan, J.H. Lienhard V, Inorganic fouling mitigation by salinity cycling in batch reverse osmosis, Water Res. 137 (2018) 384–394.
[44] Y.A. Çengel, R.H. Turner, J.M. Cimbala, M. Kanoglu, Fundamentals of Thermal-Fluid Sciences, McGraw-Hill New York, 2001.
[45] G. Rogers, Y. Mayhew, Engineering Thermodynamics Work and Heat Transfer, Prentice-Hall, 1992.
[46] G.P. Thiel, R.K. McGovern, S.M. Zubair, Thermodynamic equipartition for increased second law efficiency, Appl. Energy 118 (2014) 292–299.
[47] R.L. Stover, Industrial and brackish water treatment with closed circuit reverse osmosis, Desalin. Water Treat. 51 (2013) 1124–1130.
[48] J. Seo, Y.M. Kim, S.H. Chae, S.J. Lim, H. Park, J.H. Kim, An optimization strategy for a forward osmosis-reverse osmosis hybrid process for wastewater reuse and seawater desalination: a modeling study, Desalination 463 (2019) 40–49.
[49] J. Kim, S. Hong, A novel single-pass reverse osmosis configuration for high-purity water production and low energy consumption in seawater desalination, Desalination 429 (2018) 142–154.
[50] C.P. Koutsou, S.G. Yiantsios, A.J. Karabelas, A numerical and experimental study of mass transfer in spacer-filled channels: effects of spacer geometrical characteristics and Schmidt number, J. Membr. Sci. 326 (2009) 234–251.
[51] K. Park, H. Heo, D.Y. Kim, D.R. Yang, Feasibility study of a forward osmosis/crystallization/reverse osmosis hybrid process with high-temperature operation: modeling, experiments, and energy consumption, J. Membr. Sci. 555 (2018) 206–219.
[52] K. Park, D.Y. Kim, D.R. Yang, Cost-based feasibility study and sensitivity analysis of a new draw solution assisted reverse osmosis (DSARO) process for seawater desalination, Desalination 422 (2017) 182–193.
[53] R. Darby, R. Darby, R.P. Chhabra, Chemical Engineering Fluid Mechanics, Revised and Expanded, CRC Press, 2001.
[54] A. Haidari, S. Heijman, W. van der Meer, Visualization of hydraulic conditions inside the feed channel of reverse osmosis: a practical comparison of velocity between empty and spacer-filled channel, Water Res. 106 (2016) 232–241.
[55] D.Y. Kim, B. Gu, D.R. Yang, An explicit solution of the mathematical model for osmotic desalination process, Korean J. Chem. Eng. 30 (2013) 1691–1699.
[56] R. Timings, Mechanical Engineer's Pocket Book, Elsevier, 2005.
[57] A. Rodríguez-Calvo, G.A. Silva-Castro, F. Osorio, J. González-López, C. Calvo, Reverse osmosis seawater desalination: current status of membrane systems, Desalin. Water Treat. 56 (2015) 849–861.
[58] S.S. Shenvi, A.M. Isloor, A. Ismail, A review on RO membrane technology: developments and challenges, Desalination 368 (2015) 10–26.
[59] M. Barello, D. Manca, R. Patel, I.M. Mujtaba, Neural network based correlation for estimating water permeability constant in RO desalination process under fouling, Desalination 345 (2014) 101–111.
[60] E.M. Hoek, J. Allred, T. Knoell, B.-H. Jeong, Modeling the effects of fouling on full-scale reverse osmosis processes, J. Membr. Sci. 314 (2008) 33–49.
[61] E.M. Vrijenhoek, S. Hong, M. Elimelech, Influence of membrane surface properties on initial rate of colloidal fouling of reverse osmosis and nanofiltration membranes, J. Membr. Sci. 188 (2001) 115–128.
[62] L. Zou, I. Vidalis, D. Steele, A. Michelmore, S. Low, J. Verberk, Surface hydrophilic modification of RO membranes by plasma polymerization for low organic fouling, J. Membr. Sci. 369 (2011) 420–428.
[63] A.S. Stillwell, M.E. Webber, Predicting the specific energy consumption of reverse osmosis desalination, Water 8 (2016) 601.
[64] R. Zhao, S. Porada, P. Biesheuvel, A. Van der Wal, Energy consumption in membrane capacitive deionization for different water recoveries and flow rates, and comparison with reverse osmosis, Desalination 330 (2013) 35–41.
[65] B.A. Qureshi, S.M. Zubair, Exergetic analysis of a brackish water reverse osmosis desalination unit with various energy recovery systems, Energy 93 (2015) 256–265.
[66] A. Karabelas, C. Koutsou, M. Kostoglou, D. Sioutopoulos, Analysis of specific energy consumption in reverse osmosis desalination processes, Desalination 431 (2018) 15–21.